energies

Article

Dynamic-Depreciation-Aware Bi-Level Capacity Optimization of Shared Energy Storage for Renewable Energy Bases Considering Multi-Service Operation

Yu Wang [1], Mengyang Huang [2,*], Tianqi Xu [1,*], Jindi Zhang [2] and Pengfei Li [3]

[1] School of Electrical and Information Engineering, Yunnan Minzu University, Kunming 650504, China; 24214037870036@ymu.edu.cn
[2] School of Metallurgy and Materials Engineering, Department of Metallurgy, Honghe University, Mengzi 661199, China; zhangjindi@uoh.edu.cn
[3] Yunnan Key Laboratory of Unmanned Autonomous Systems, Kunming 650504, China; 24214037870022@ymu.edu.cn
* Correspondence: huangmengyang@uoh.edu.cn (M.H.); xu.tianqi@ymu.edu.cn (T.X.)

Abstract

Shared energy storage (SES) in renewable energy bases can integrate reliability support, curtailed-energy accommodation, spot-market arbitrage, and frequency-regulation services, but unclear service boundaries and static depreciation may distort capacity-allocation and economic-evaluation results. This paper proposes a bi-level capacity optimization model that incorporates operational intensity and dynamic depreciation. The model defines service-occupation boundaries and cycle-attribution rules, uses annual equivalent cycles to quantify cycling intensity, and feeds this intensity back into economic lifetime and capacity-side depreciation, forming a closed loop of capacity configuration, operational dispatch, lifetime assessment, and cost correction. A seasonal representative-day case study shows that static depreciation overestimates annualized net income by 7.55% under the same configuration. The dynamic-depreciation closed loop corrects the evaluation of high-cycling schemes and identifies leasing-based reliability support, passive curtailed-energy accommodation, and spot-market arbitrage as the preferred scheme under the benchmark conditions. Passive accommodation reduces annual curtailed energy by 54.90% and increases annualized net income by 41.40%. The proposed method provides a quantitative basis for capacity configuration and multi-service operation of shared energy storage in renewable energy bases.

Keywords: shared energy storage; renewable energy base; capacity configuration; annual equivalent cycles; dynamic depreciation; bi-level optimization

Check for updates

Academic Editor: Andrea De Pascale

Received: 3 June 2026
Revised: 2 July 2026
Accepted: 10 July 2026
Published: 14 July 2026

1. Introduction

With the continued advancement of the "Dual Carbon" goals, the installed capacity of renewable energy represented by wind power and photovoltaic power has grown rapidly, and renewable energy bases and clusters have become an important direction for the low-carbon transformation of power systems [1]. Compared with conventional power sources, renewable energy output is characterized by randomness, volatility, and counter-peak regulation features. When large-scale renewable energy is centrally connected to the grid, mismatches among renewable output, load demand, transmission-channel capacity, and system regulation capability may cause wind and solar curtailment, grid-connection constraints, and insufficient operational flexibility [2,3]. Energy storage systems,

 https://doi.org/10.3390/en19143311

owing to their fast charging and discharging capability, energy time-shifting function, and bidirectional regulation characteristics, have become an important technical means to improve renewable energy accommodation, enhance system flexibility, and support the construction of new power systems.

Conventional energy storage configuration is generally dominated by self-built and self-used systems for individual renewable energy stations. However, in renewable energy base scenarios, the output fluctuations, curtailment periods, and regulation requirements of different wind farms and photovoltaic stations are not completely consistent. Independent configuration at each station may therefore lead to duplicated investment, redundant capacity, and insufficient equipment utilization. Shared energy storage, through centralized construction, unified operation, and multi-entity sharing, transforms energy storage resources from dedicated station-side assets into public regulation resources serving multiple renewable energy entities [4]. Existing studies have examined shared energy storage from several perspectives, including capacity planning, coordinated operation of station clusters [5,6], leasing mechanisms, spot-market arbitrage, ancillary-service participation, and degradation-aware evaluation [7,8].

As shared energy storage shifts from single-function operation to joint multi-service operation, its capacity configuration and dispatch become more strongly coupled [9,10]. Leasing-based reliability support, passive accommodation of curtailed renewable energy, spot-market arbitrage, and frequency-regulation ancillary services occupy power capacity, energy capacity, and state-of-charge (SOC) space in different ways [11]. If service boundaries are not explicitly defined, reliability-support resources may be crowded out by market-oriented dispatch, and conflicts may arise among accommodation space, arbitrage space, and frequency-regulation reserves. Meanwhile, multi-service stacking increases cycling intensity and may accelerate battery degradation [12–14]. Capacity configuration models based on fixed-lifetime or static-depreciation assumptions may therefore overestimate the long-term economic performance of high-cycling operation schemes.

In summary, although existing studies have addressed the multi-scenario configuration and diversified revenue evaluation of shared energy storage, several limitations remain. First, the allocation of power-capacity space and service priorities among stacked services has not been clearly characterized, making it difficult to reflect resource-occupation boundaries in joint operation. Second, lifetime degradation is often treated using fixed depreciation periods or fixed cycling costs, without feeding actual operating intensity back into the economic lifetime and capacity-side depreciation cost. Third, the closed-loop mechanism among service boundaries, operating intensity, lifetime depreciation, and capacity configuration has not been sufficiently characterized [15,16]. Therefore, it remains difficult to jointly evaluate the effects of multi-service revenue improvement, curtailed-energy accommodation enhancement, and lifetime-depreciation cost variation on capacity configuration results.

To address the above issues, this paper develops a bi-level optimal configuration method for shared energy storage in renewable energy bases under multi-service operation, considering operational intensity and dynamic depreciation. First, service-occupation boundaries and cycle-attribution rules are clarified under the principle of "reserve priority, idle-space accommodation, and residual market-based dispatch". Second, annual equivalent cycles are used to quantify the operational intensity of shared energy storage and to connect service-specific cycling contributions with lifetime assessment. Third, operational intensity is fed back into the actual economic lifetime and capacity-side dynamic depreciation cost, forming a closed-loop capacity optimization framework solved by Dung Beetle Optimizer (DBO) and Mixed-integer linear programming (MILP) [17]. Seasonal representative-day case studies further verify the proposed method through dynamic-depreciation model comparison, multi-service scheme selection, operational-mechanism verification, and parameter sensitivity analysis. The results show that dynamic depreciation can correct the overestimation of high-cycling schemes and support economically robust multi-service operation decisions for shared energy storage in renewable energy bases. Compared with existing studies that mainly focus on shared energy storage scheduling, multi-service revenue evaluation, degradation-aware dispatch, or fixed cycling-cost representation, the present study further emphasizes the closed-loop interaction between service-boundary allocation, service-specific cycling intensity, economic lifetime correction, and capacity configuration. The methodological novelty of this paper therefore lies in the integration of four linked elements. First, the power-capacity, SOC-feasibility, and cycle-attribution boundaries of leasing-based reliability support, passive curtailed-energy accommodation, spot-market arbitrage, and frequency-regulation services are explicitly separated. Second, a service-specific cycle-attribution logic is established to avoid double counting of cycling contributions under multi-service stacking. Third, annual equivalent cycles are fed back into the actual economic lifetime and the annualized capacity-side dynamic depreciation cost, so that high-cycling configurations are economically corrected during capacity planning rather than only evaluated after dispatch. Finally, the above mechanisms are embedded into a bi-level configuration-dispatch framework, in which upper-level capacity decisions and lower-level representative-day operation interact through revenue, curtailed energy, cycling intensity, lifetime, and depreciation-cost feedback.

2. Operation Mode of Shared Energy Storage in Renewable Energy Bases

2.1. Multi-Service Coordinated Operation Framework

Shared energy storage for renewable energy bases simultaneously undertakes reliability-support services, accommodation services, and market-oriented services [18,19]. In this paper, the operation process is divided into four service segments: leasing-based reliability support, passive accommodation of curtailed renewable energy, spot-market arbitrage, and frequency-regulation ancillary services. The operating principle of "reserve priority, idle-space accommodation, and residual market-based dispatch" is adopted. Specifically, the resources reserved for leasing are first used to satisfy reliability-support dispatch, and their idle part can be used for passive accommodation of curtailed renewable energy. Spot-market arbitrage only uses the remaining adjustable space after deducting leasing reserves and frequency-regulation reserves, while frequency-regulation services participate in the ancillary service market by reserving part of the converter power capacity.

It should be noted that passive accommodation of curtailed renewable energy is not an independent chargeable service, but an accommodation function undertaken when leasing-based reliability-support resources are idle. The leased power belongs to the reliability-support reserve capacity committed to renewable energy stations, rather than freely dispatchable market-oriented arbitrage power. Therefore, the multi-service operation boundaries of shared energy storage are divided into three categories [20,21]. The first is the power-occupation boundary, in which leasing-based reliability-support power and frequency-regulation reserve power occupy converter capacity with priority, and spot-market arbitrage only uses the remaining power after these reserves are deducted. The second is the SOC feasibility boundary, in which passive accommodation and reliability-support dispatch must satisfy the SOC upper and lower limits and the initial-terminal SOC closure constraint in Equation (23). Before entering the lower-level optimization, the exogenous reliability-support dispatch curve must be checked for power and SOC feasibility. The third is the cycle-attribution boundary, which distinguishes leasing-related cycles, spot-market arbitrage cycles, and frequency-regulation cycles according to service channels. No explicit SOC reserve variable is further introduced in this paper, and frequency-regulation responses are treated as zero-mean disturbances at the day-ahead dispatch timescale.

To further illustrate the stakeholder relationships and service boundaries of shared energy storage in renewable energy bases, an operational framework is developed, as shown in Figure 1.

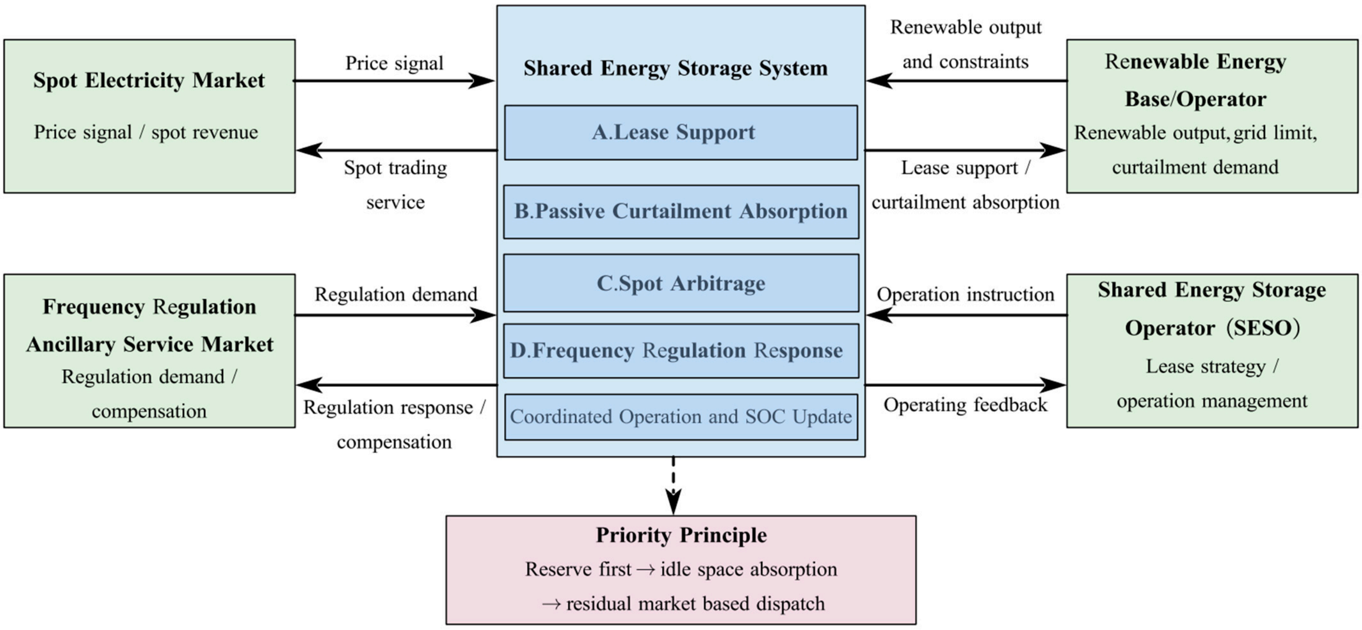

Figure 1. Operational framework of shared energy storage in a renewable energy base. The blue, green, and pink boxes denote the shared-energy-storage operation module, external stakeholders/markets, and the priority principle, respectively; the dashed arrow indicates that the priority principle guides the coordination of the service modules.

As shown in Figure 1, the shared energy storage system is positioned among the renewable energy base, the spot electricity market, the frequency-regulation ancillary service market, and the shared energy storage operator. The renewable energy base provides renewable output, grid-connection constraints, and curtailed-energy accommodation demand. The spot market provides price signals for arbitrage operations, and the frequency-regulation ancillary service market provides regulation requirements and compensation mechanisms. The shared energy storage operator is responsible for leasing strategy formulation and operational management, thereby coordinating multi-stakeholder resource allocation.

2.2. Service Boundaries and Cycle-Attribution Logic

Based on the above multi-service operation boundaries, this paper further clarifies the cycle-attribution relationships among different services to avoid double counting of cycling degradation under joint multi-service operation [22]. Leasing-related cycles include the cycles caused by periodic testing, routine maintenance, reliability-support dispatch, and passive accommodation of curtailed renewable energy undertaken by idle leased resources. Spot-market arbitrage cycles are formed by active charging and discharging behaviors driven by market price signals, while frequency-regulation cycles are formed by frequency-regulation response power.

Although passive accommodation of curtailed renewable energy is treated as an independent operational segment in the service-boundary division, it uses the idle power and SOC space of leasing-based reliability-support resources when they are not called upon, rather than being an active market-arbitrage behavior based on electricity price signals. Therefore, in the cycling-degradation accounting adopted in this paper, the cycle contribution generated by passive accommodation is attributed to leasing-related cycles and is not included in spot-market arbitrage cycles. This attribution rule provides the statistical basis for annual equivalent-cycle calculation and dynamic-depreciation feedback in the subsequent model.

3. Operational-Intensity Characterization and Bi-Level Optimization Model for Shared Energy Storage

3.1. Operational-Intensity Characterization and Calculation of Annual Equivalent Cycles

To characterize the utilization level of shared energy storage under different service combinations, this paper adopts the annual equivalent number of cycles as the operational-intensity indicator [23]. This indicator can uniformly map the charge–discharge utilization levels in representative-day dispatch, arbitrage operation, and ancillary-service participation to the lifetime assessment and depreciation-cost correction processes. To establish a unified metric for degradation quantification under different service modes, this paper characterizes the operational intensity of energy storage using an equivalent-cycle conversion criterion based on available capacity. Considering that the revenue from spot-market arbitrage is mainly realized through grid-injected discharge energy, and that the existing case studies in this paper calculate arbitrage cycles based on discharge-side energy, the arbitrage equivalent cycles of representative days are defined as discharge-side equivalent cycles.

$$n_{arbi,s} = \frac{\sum_{t=1}^{24} P_{dis,s}^{arbi}(t) \cdot \Delta t}{\eta_{dis} \cdot E \cdot (SOC_{max} - SOC_{min})} \tag{1}$$

where $P_{dis,s}^{arbi}(t)$ denotes the arbitrage discharging power decided in time period t of representative day s, MW; Δt is the dispatch time step, which is set to 1 h; E denotes the rated energy capacity of the energy storage system, MWh; SOC_{max} and SOC_{min} denote the upper and lower limits for safe operation, respectively, which are set to 0.9 and 0.1; and η_{dis} denotes the discharging efficiency.

For leasing services, let F_{test} denote the annual number of tests, DOD_{test} denote the depth of discharge per test, $n_{maint,day}$ denote the equivalent number of cycles for daily maintenance, and ω_s denote the annualization weight of representative day s. For leasing-related cycles, this paper adopts a charge–discharge throughput-based conversion approach, in which the discharged energy from reliability-support dispatch and the charged energy from passive accommodation are converted into the equivalent number of cycles for the representative day:

$$\begin{cases} n_{disp,s} = \dfrac{\sum_{t=1}^{24} \left[\frac{P_{dis,s}^{lease}(t)}{\eta_{dis}} + \eta_{ch} P_{ch,s}^{abs}(t) \right] \Delta t}{2E \cdot (SOC_{max} - SOC_{min})} \\ N_{lease} = F_{test} \cdot DOD_{test} + 365 \left(n_{maint,day} + \sum_{s=1}^{S} \omega_s \cdot n_{disp,s} \right) \end{cases} \tag{2}$$

where $n_{disp,s}$ denotes the equivalent number of cycles jointly formed by leasing-based reliability-support discharging and passive accommodation using idle leased resources on representative day s; $P_{dis,s}^{lease}(t)$ denotes the discharging power for leasing-based reliability-support dispatch, and $P_{ch,s}^{abs}(t)$ denotes the charging power for passive accommodation of curtailed renewable energy; η_{ch} denotes the charging efficiency. The denominator $2E \cdot (SOC_{max} - SOC_{min})$ represents the effective energy throughput corresponding to one complete charge–discharge cycle. N_{lease} denotes the leasing-related annual equivalent number of cycles, which consists of annual testing cycles, daily maintenance cycles, and the weighted reliability-support dispatch and passive accommodation cycles of the four seasonal representative days.

If the arbitrage equivalent cycles of representative days are calculated using Equation (1), the annual equivalent cycles contributed by spot-market arbitrage can be expressed as follows:

$$N_{arbi} = 365\sum_{s=1}^{S} \omega_s \cdot n_{arbi,s} \tag{3}$$

where $n_{arbi,s}$ is calculated using Equation (1), with the unit of cycles/day.

Frequency-regulation services are characterized by high-frequency and shallow charge–discharge operation, and the corresponding cycling degradation can be converted into equivalent cycles through time-domain integration of the response power. It should be noted that Equation (4) is used only to convert frequency-regulation response mileage into equivalent cycling degradation. In this paper, the frequency-regulation response is assumed to be an approximately zero-mean bidirectional disturbance at the day-ahead energy dispatch timescale, and therefore it does not change the day-ahead SOC energy balance in Equation (23). The equivalent regulation-response power $P_{reg,s}(t)$ is constructed to represent the cycling effect of frequency-regulation participation at the representative-day scale. It should be distinguished from the declared regulation reserve capacity P_{freq}. In the benchmark case, $P_{reg,s}(t)$ is represented by an approximately zero-mean bidirectional response sequence, and its response mileage is scaled according to the declared frequency-regulation capacity and the mileage-to-capacity parameter. Therefore, $P_{reg,s}(t)$ is used only for equivalent-cycle conversion, whereas P_{freq} is used for reserve-capacity occupation and frequency-regulation revenue calculation. If the actual frequency-regulation signal has a persistent energy bias, the frequency-regulation energy term should be further incorporated into the SOC dynamic constraints. If the equivalent frequency-regulation response power in time period t of representative day s is $P_{reg,s}(t)$, and the reference depth of discharge is DOD_{ref}, the annual equivalent cycles contributed by frequency-regulation services can be expressed as follows:

$$N_{freq} = 365\sum_{s=1}^{S} \omega_s \cdot \sum_{t=1}^{24} \frac{\left|P_{reg,s}(t)\right| \cdot \Delta t}{2E \cdot (SOC_{max} - SOC_{min}) \cdot DOD_{ref}} \tag{4}$$

It should be noted that P_{freq} denotes the declared frequency-regulation capacity or frequency-regulation reserve power in Equations (12) and (22). It is used for frequency-regulation revenue calculation and power-reservation boundary setting and does not directly replace $P_{reg,s}(t)$ in the cycle conversion. In the benchmark case, DOD_{ref} is set to 0.10, representing the reference shallow-cycle depth used for converting high-frequency regulation mileage into equivalent cycles rather than the actual depth of every regulation movement. The zero-mean assumption implies that the positive and negative regulation energies are approximately balanced over the day-ahead dispatch interval; therefore, frequency-regulation participation mainly affects the equivalent-cycle calculation and does not change the SOC trajectory in Equation (23). If the actual regulation signal contains a persistent energy bias, the SOC trajectory may drift upward or downward. In that case, the regulation-related charging or discharging energy should be explicitly included in the SOC dynamic constraint, and additional SOC reserve may be required to maintain feasibility. Such a case may reduce the available energy space for passive accommodation and spot-market arbitrage, and may also lead to a larger optimal energy capacity or a more conservative service-reservation strategy.

If high-resolution regulation data are available, the equivalent regulation-response power in Equation (4) can be replaced by the measured second-level or minute-level regulation trajectory, and the equivalent-cycle calculation can be performed by integrating the measured regulation mileage over the dispatch interval. In this case, the cycling contribution of frequency regulation can be evaluated more accurately. If the high-resolution signal has a nonzero cumulative energy deviation, the corresponding net regulation energy should also be incorporated into the SOC dynamic constraint, rather than being treated only as an equivalent-cycle term.

The high-frequency shallow charge–discharge behavior is uniformly converted into equivalent cycles. It should be noted that Equations (1), (2) and (4) are all business-channel-based statistical criteria for equivalent cycles, which are used to convert the operational intensity caused by different services into a unified annual equivalent cycle indicator. Since different services share the same SOC state variable, this paper does not further track the energy-source attribution of passively accommodated energy in subsequent discharging channels. Instead, the cycle contributions are approximately counted according to power channels. On this basis, the annual equivalent number of cycles of shared energy storage under joint multi-service operation can be expressed as follows:

$$N_{real} = N_{lease} + N_{arbi} + N_{freq} \tag{5}$$

The N_{real} obtained from Equation (5) is used as an input variable for economic lifetime assessment and dynamic depreciation calculation.

To examine the sensitivity to the cycle-attribution rule, it should be noted that the benchmark attribution rule mainly affects the service-specific decomposition of annual equivalent cycles. In this paper, passive curtailed-energy accommodation is attributed to leasing-related cycles because it uses idle leased resources rather than price-driven arbitrage resources. If the same passive-accommodation throughput is only reclassified from leasing-related cycles to arbitrage-related cycles while keeping the same equivalent-cycle conversion denominator, the total annual equivalent cycles in Equation (5) remain unchanged. Therefore, the actual economic lifetime, capacity-side dynamic depreciation cost, and optimized capacity configuration are not affected by this pure service-label reclassification. However, if a different equivalent-cycle conversion basis is adopted, such as replacing discharge-side arbitrage cycles with full charge–discharge throughput cycles, the total annual equivalent cycles may change. This case requires more detailed battery ageing data and is therefore regarded as a limitation and a future extension of the present planning-level economic depreciation model.

3.2. Economic Lifetime Assessment and Dynamic Depreciation Mechanism

Under the fixed-lifetime depreciation assumption, the annualized cost of an energy storage system is usually not adjusted for changes in operational intensity, which may lead to an overestimation of the long-term economic performance of high-cycling operation schemes [24,25]. To reflect the impact of actual operation levels on lifetime degradation, this paper defines the actual economic lifetime of the energy storage battery as the smaller value between its cycle life and calendar life, namely:

$$L_{real} = \begin{cases} L_{cal}, N_{real} \le \frac{N_{ref}}{L_{cal}} \\ \frac{N_{ref}}{N_{real}}, N_{real} > \frac{N_{ref}}{L_{cal}} \end{cases} \tag{6}$$

where L_{real} denotes the actual economic lifetime of the energy storage system; L_{cal} denotes the calendar life; N_{ref} denotes the reference cycle life of the battery; and N_{real} denotes the annual equivalent number of cycles. When the annual equivalent number of cycles does not exceed N_{ref}/L_{cal}, the lifetime of the energy storage system is mainly limited by the calendar life, and the actual economic lifetime is set to L_{cal}. When the annual equivalent number of cycles exceeds N_{ref}/L_{cal}, the lifetime of the energy storage system is mainly limited by the cycle life, and the actual economic lifetime is calculated as N_{ref}/N_{real}.

Based on the economic lifetime assessment, this paper further converts the capacity-side investment cost into a dynamic depreciation cost using an annuity-based annualization method, so as to reflect the actual annualized cost of capacity configuration schemes under different operating levels [26]. The capacity-side dynamic depreciation cost can be expressed as follows:

$$C_{dep,real} = \frac{r(1+r)^{L_{real}}}{(1+r)^{L_{real}} - 1} \cdot \alpha E \tag{7}$$

where $C_{dep,real}$ denotes the capacity-side dynamic annualized depreciation cost; r denotes the benchmark discount rate; and α denotes the unit energy-capacity investment cost, 10^4 CNY/MWh. This equation enables the capacity-side annualized depreciation cost to be dynamically adjusted with N_{real} and imposes a stronger economic constraint on high-cycling operation schemes. In this paper, the dynamic depreciation correction is introduced only for the capacity-side investment cost, while the power-side investment cost is still annualized based on a fixed lifetime. It should be emphasized that the proposed formulation is a cycle-intensity-adjusted economic depreciation model rather than a full electrochemical battery degradation model. The annual equivalent number of cycles is used to represent the overall cycling intensity caused by multi-service operation and to update the actual economic lifetime and the annualized capacity-side depreciation cost. Therefore, the model captures the economic consequence of cycling intensity in capacity planning, but it does not explicitly describe detailed electrochemical ageing mechanisms, such as temperature dependence, C-rate effects, variable depth-of-discharge ageing, SOC-dependent calendar ageing, or time-dependent capacity fade. These factors can be incorporated in future work by replacing the equivalent-cycle-based lifetime function with a more detailed state-of-health degradation model.

The sensitivity of the dynamic depreciation correction is mainly governed by the reference cycle life N_{ref}, the calendar life L_{cal}, and the threshold N_{ref}/L_{cal}. When N_{real} does not exceed this threshold, the economic lifetime is calendar-life-limited and is set to L_{cal}. When N_{real} exceeds this threshold, the economic lifetime becomes cycle-life-limited and is calculated as N_{ref}/N_{real}. Therefore, a larger N_{ref} raises the threshold for cycle-life limitation and weakens the depreciation penalty caused by high cycling intensity, whereas a smaller N_{ref} strengthens the dynamic depreciation correction. Changes in L_{cal} affect both the calendar-life cap and the transition threshold between calendar-life-limited and cycle-life-limited operation. Accordingly, the numerical results should be interpreted under the benchmark lifetime parameters adopted in the case study.

3.3. Bi-Level Optimization Model Structure and Information Interaction

There is a bidirectional coupling relationship between the capacity configuration and operational dispatch of shared energy storage. On the one hand, the upper-level capacity configuration determines the power capacity, energy capacity, and service-reservation boundaries for lower-level representative-day dispatch. On the other hand, the lower-level dispatch results affect spot-market arbitrage revenue, curtailed energy, and the annual equivalent number of cycles, thereby changing the upper-level economic evaluation. To characterize the above coupling relationship, this paper develops a bi-level optimization model with "upper-level capacity configuration–lower-level representative-day dispatch" [27].

The upper-level model aims to maximize the annualized net income of shared energy storage and determines the rated power P and rated energy capacity E of the energy storage system. For each candidate capacity configuration, the upper-level transfers P, E, and the service-reservation boundaries to the lower-level model. The lower level then returns the representative-day dispatch results to the upper level for annualized net income evaluation and dynamic depreciation correction. The calculation of specific feedback variables is described in Section 3.6.

Given P, E, and the service-reservation boundaries, the lower-level model takes the maximization of spot-market arbitrage revenue as the primary objective and uses curtailed-energy minimization with a small weight as a tie-breaking term for equivalent optimal solutions [28]. The model determines the 24 h operating strategy, and its formulation can be expressed as follows:

$$y_s^* = arg\ max_{y_s}\ \pi_{day,s}(y_s|P,E),s = 1,2,\cdots S \tag{8}$$

where y_s^* denotes the set of optimal lower-level dispatch decision variables corresponding to representative day s. The variable set y_s includes the charging and discharging power for spot-market arbitrage, the charging power for passive accommodation of curtailed renewable energy, the discharging power for leasing-based reliability-support dispatch, curtailed power, grid-connected power, charging and discharging status variables, and SOC. $\pi_{day,s}(y_s|P,E)$ denotes the lower-level dispatch objective value of representative day s under the rated power P and rated energy capacity E given by the upper level. S denotes the total number of representative days.

This paper adopts a hierarchical solution architecture of "DBO + MILP". In the upper level, DBO is used to search for candidate capacity configurations, while in the lower level, MILP is used to solve the representative-day dispatch problem [29].

DBO is adopted as a derivative-free upper-level search method because the upper-level fitness value is obtained through a nested evaluation process. For each candidate P/E configuration, the lower-level MILP dispatch problem must be solved first, and the resulting dispatch variables are then used to calculate annual equivalent cycles, actual economic lifetime, dynamic depreciation cost, and annualized net income. This nested mapping from the capacity decision variables to the upper-level objective is non-smooth and implicit, and is therefore not directly suitable for conventional gradient-based deterministic optimization. In contrast, the lower-level dispatch problem remains a deterministic MILP under a given capacity configuration. It should also be emphasized that this paper does not aim to prove the universal superiority of DBO over other metaheuristic algorithms. Other derivative-free metaheuristics or enumeration-based searches can be coupled with the proposed modelling framework when computational cost is acceptable. The independent-run stability test in Table A5 is used to evaluate the computation time and convergence stability of the adopted DBO search in the benchmark case.

To improve the reproducibility of the proposed DBO–MILP solution procedure, the computational implementation settings are summarized in Table A4. In the upper-level capacity search, the Dung Beetle Optimizer (DBO) is applied to the two-dimensional decision vector ([P,E]), with the annualized net income as the fitness function. The population size is set to 18, and the maximum number of iterations is set to 30. Candidate capacity solutions are repaired according to the power-capacity bounds, energy-capacity bounds, E/P ratio bounds, and 1 MW/1 MWh discretization steps, while investment-budget and annual-cycle-limit violations are handled using penalty terms. For each candidate capacity configuration, the lower-level 24 h dispatch model is formulated as a mixed-integer linear programming (MILP) problem and solved in MATLAB R2022b, 64-bit Windows using intlinprog in the reported experiments.

To examine the influence of metaheuristic randomness, the benchmark M3 case was repeated for 10 independent DBO runs with different random seeds. As shown in Table A5, all 10 independent runs obtained the same optimal configuration of P* = 180 MW and E* = 720 MWh. The coefficient of variation of the annualized net income was only 2.18×10^{-14}%, indicating that the objective values were almost identical across different random seeds. The average computation time was 75.81 s with a standard deviation of 1.67 s. These results indicate that the upper-level DBO search provides stable optimal or near-optimal solutions for the benchmark configuration problem. The dispatch results are then fed back to the upper level for dynamic depreciation correction and candidate-solution updating. To illustrate the information transfer and iterative updating relationship between the upper and lower levels, this paper develops a bi-level optimization solution procedure for shared energy storage in a renewable energy base, as shown in Figure 2.

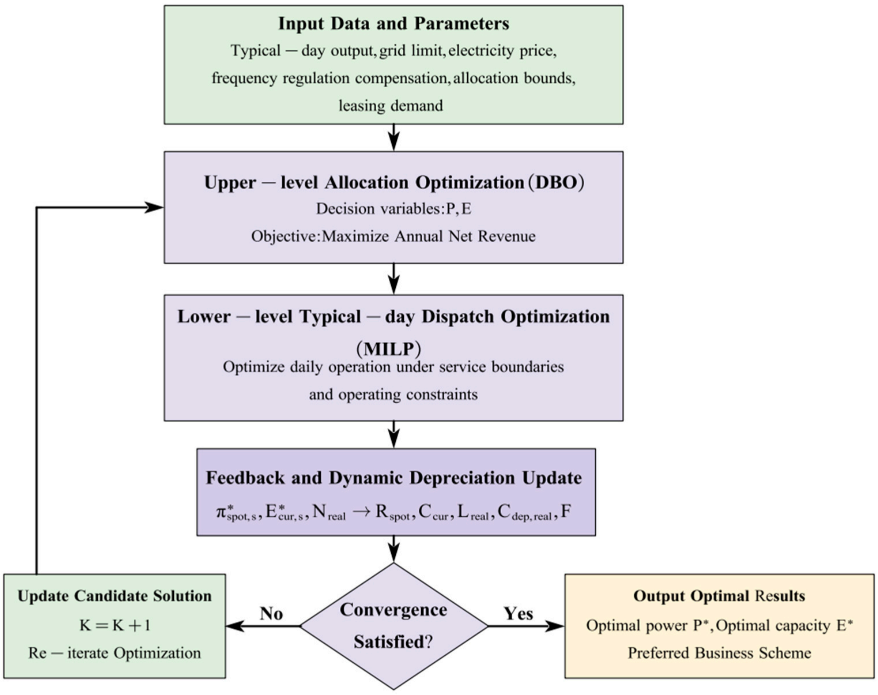

Figure 2. Bi-level optimization solution procedure for shared energy storage in a renewable energy base.

As shown in Figure 2, the solution procedure uses candidate capacity configurations as the interface between the upper and lower levels. The representative-day dispatch results from the lower level are fed back to the upper level, and the iterative optimization of capacity configuration is completed through dynamic depreciation correction and convergence judgment.

3.4. Upper-Level Capacity Configuration Model

3.4.1. Upper-Level Objective Function and Revenue–Cost Components

The upper-level capacity configuration model aims to maximize the annualized net income of shared energy storage, with the rated power P and rated energy capacity E as decision variables. The objective function comprehensively considers leasing revenue, spot-market arbitrage revenue, frequency-regulation revenue, fixed annualized investment cost on the power side, system operation and maintenance costs, capacity-side dynamic depreciation cost, and curtailed-energy penalty cost:

$$max_{P,E}F = R_{lease} + R_{spot} + R_{freq} - \left[C_{fix} + C_{dep,real} + C_{cur}\right] \tag{9}$$

where F denotes the annualized net income, 10^4 CNY/year; R_{lease}, R_{spot}, and R_{freq} denote the annual revenues from leasing, spot-market arbitrage, and frequency-regulation ancillary services, respectively; and C_{fix}, $C_{dep,real}$, and C_{cur} denote the fixed annualized power-side investment and system operation and maintenance cost, the dynamically corrected capacity-side depreciation cost, and the curtailed-energy penalty cost, respectively.

The detailed calculations of each revenue and cost component are as follows:

(1) Annual Leasing Revenue

Shared energy storage obtains fixed revenue by providing reliability-support reserve capacity to renewable energy stations. The revenue is charged based on the reserved power and energy-capacity resources, rather than the actual discharged energy. Therefore, the leasing revenue can be expressed as follows:

$$\begin{cases} P_{lease} = K_{lease,P} \cdot P \\ E_{lease} = K_{lease,E} \cdot E \\ R_{lease} = \lambda_{lease,P} \cdot P_{lease} + \lambda_{lease,E} \cdot E_{lease} \end{cases} \tag{10}$$

where $\lambda_{lease,P}$ and $\lambda_{lease,E}$ denote the unit leasing prices of power and energy capacity, respectively, 10^4 CNY/MW/year and 10^4 CNY/MWh/year; and $K_{lease,P}$ and $K_{lease,E}$ denote the leasing ratios of power and energy capacity, respectively.

(2) Annual Spot-Market Arbitrage Revenue

The annual spot-market arbitrage revenue is obtained by annualizing the representative-day net spot-market arbitrage revenue derived from the lower-level day-ahead dispatch model, namely:

$$\begin{cases} \pi^*_{spot,s} = \sum_{t=1}^{24} \pi_s(t) \left[P^{arbi,*}_{dis,s}(t) - P^{arbi,*}_{ch,s}(t) \right] \Delta t \\ R_{spot} = 365 \sum_{s=1}^{S} \omega_s \cdot \pi^*_{spot,s} \end{cases} \tag{11}$$

where $\pi^*_{spot,s}$ denotes the net spot-market arbitrage revenue obtained for representative day s under the optimal dispatch solution y_s^*; $\pi_s(t)$ denotes the spot electricity price in time period t; and $P^{arbi,*}_{dis,s}(t)$ and $P^{arbi,*}_{ch,s}(t)$ denote the spot-market arbitrage discharging and charging power under the optimal solution, respectively. It should be noted that $\pi^*_{spot,s}$ in Equation (11) represents the net spot-market arbitrage revenue and does not include the ε-weighted curtailed-energy tie-breaking term in Equation (19).

(3) Annual Revenue from Frequency-Regulation Ancillary Services

When shared energy storage participates in frequency-regulation ancillary services, its revenue is mainly related to the declared frequency-regulation capacity, unit capacity compensation level, frequency-regulation response mileage, and response performance [30]. To characterize the impact of frequency-regulation services on the annualized revenue of shared energy storage, this paper expresses the frequency-regulation revenue as a combined form of capacity compensation and mileage compensation:

$$\begin{cases} P_{freq} = K_{freq} \cdot P \\ R_{freq} = 8760 \cdot P_{freq} \cdot \left(\lambda^M_{cap} + \lambda^M_{mil} \cdot K_m \right) \cdot K_{perf} \end{cases} \tag{12}$$

where P_{freq} denotes the declared frequency-regulation capacity, MW; K_{freq} denotes the frequency-regulation power reservation ratio; λ^M_{cap} denotes the frequency-regulation capacity compensation price, 10^4 CNY/MWh; λ^M_{mil} denotes the frequency-regulation mileage compensation price, 10^4 CNY/MWh; K_m denotes the regulation mileage-to-capacity ratio; and K_{perf} denotes the frequency-regulation performance coefficient of energy storage. Since the compensation mechanisms for frequency-regulation ancillary services vary across regions, the above parameters are used only as benchmark market parameters in this paper to analyze the impact of changes in frequency-regulation service revenue on the optimal business-scheme selection of shared energy storage.

(4) Fixed Annualized Power-Side Investment Cost and System Operation and Maintenance Cost

$$C_{fix} = \frac{r(1+r)^n}{(1+r)^n - 1} \cdot (\beta P) + \omega \cdot (\alpha E + \beta P) \tag{13}$$

where the first term represents the fixed annualized cost of power-side equipment investment, with $n = 15$ years denoting the benchmark lifetime of the power equipment. β denotes the unit power investment cost, 10^4 CNY/MW. The second term represents the annual operation and maintenance cost of the energy storage system, which is accrued as a certain proportion of the total investment. Therefore, it includes both capacity-side and power-side investments, namely $\omega \cdot (\alpha E + \beta P)$, where ω denotes the annual operation and maintenance rate. It should be noted that αE in Equation (13) is used only to accrue capacity-related operation and maintenance costs and does not correspond to the annualized depreciation of capacity capital.

(5) Capacity-Side Dynamic Depreciation Cost

In the conventional static model, the capacity-side depreciation cost C_{dep} is calculated using a fixed depreciation period of $n = 15$ years. In this paper, the actual economic lifetime L_{real} is dynamically corrected based on the actual annual equivalent cycles N_{real} fed back from the lower level, and the capacity-side dynamic depreciation cost $C_{dep,real}$ is calculated according to Equation (7).

(6) Annualized Curtailed-Energy Penalty Cost

The curtailed-energy penalty cost is obtained by converting the total curtailed energy of representative days fed back from the lower level into an annual value using the corresponding weights, namely:

$$C_{cur} = 365 \cdot \lambda_{cur} \sum_{s=1}^{S} \omega_s \cdot E^*_{cur,s} \tag{14}$$

where $E^*_{cur,s}$ denotes the total curtailed energy of representative day s, MWh/day; λ_{cur} denotes the unit curtailed-energy penalty cost, 10^4 CNY/MWh.

3.4.2. Upper-Level Constraints

To ensure that the capacity configuration of shared energy storage is both physically and economically feasible, the following constraints are imposed in the upper-level model.

(1) Capacity Configuration Boundary Constraints

The power and energy capacity configurations of shared energy storage are constrained by the grid-connection access capability and the engineering feasibility range.

$$P_{min} \le P \le P_{max}, E_{min} \le E \le E_{max} \tag{15}$$

where P_{max} and P_{min} denote the upper and lower bounds of the power configuration, respectively; and E_{max} and E_{min} denote the upper and lower bounds of the energy capacity configuration, respectively.

(2) Project Investment Budget Constraint

The total investment of shared energy storage shall not exceed the upper limit of the project planning budget.

$$\alpha E + \beta P \le Budget_{total} \tag{16}$$

where $Budget_{total}$ denotes the maximum planned investment budget of the project, 10^4 CNY.

(3) Economic Acceptability Constraint for Leasing

The leasing price of shared energy storage should satisfy the economic acceptability requirement of renewable energy stations; that is, the leasing cost should not be higher than the smaller value between the self-built energy storage cost and the curtailed-energy loss without energy storage configuration [31,32]:

$$\begin{cases} C_{lease} \leq min\left(C_{self}, C_{loss}\right) \\ C_{lease} = \lambda_{lease,P} \cdot P_{lease} + \lambda_{lease,E} \cdot E_{lease} \\ C_{self} = \left(\frac{r(1+r)^n}{(1+r)^n - 1} + \omega\right) \cdot (\delta_E E_{lease} + \delta_P P_{lease}) \\ C_{loss} = E_{ren} \cdot \sigma_{curt} \cdot \left(\lambda_{grid} + \lambda_{fine}\right) \\ \delta_E = K_E \cdot \alpha, \delta_P = K_P \cdot \beta \end{cases} \tag{17}$$

where the expressions in Equation (17) correspond to the leasing cost paid by renewable energy stations, the annualized cost of self-built energy storage, and the comprehensive economic loss caused by curtailment, respectively. C_{self} denotes the cost of self-built energy storage for renewable energy stations, where P_{lease} and E_{lease} denote the leased power and energy capacity, respectively, and n is consistent with the calendar-life setting in Table 1. δ_E and δ_P denote the unit energy-capacity and unit power investment costs of self-built energy storage for renewable energy stations, respectively, satisfying $\delta_E = K_E \cdot \alpha$ and $\delta_P = K_P \cdot \beta$, with units of 10^4 CNY/MWh and 10^4 CNY/MW, respectively. K_E and K_P are dimensionless cost coefficients for self-built energy storage, and their values are listed in Table A3. C_{loss} denotes the annual curtailed-energy loss caused by the absence of energy storage configuration, where $E_{ren} = P_{ren} \cdot h_{ren}$ is the theoretical annual generation, P_{ren} is the installed capacity of the renewable energy station, and h_{ren} is the annual utilization hours. σ_{curt} denotes the curtailment rate, λ_{grid} denotes the unit on-grid electricity price, and λ_{fine} denotes the unit curtailment penalty. This constraint is used to ensure that the pricing of shared energy storage remains within the acceptable range of renewable energy stations.

Table 1. Key parameter settings of the case study.

Symbol	Value
r	0.08
L_{cal}	15 years
N_{ref}	6000 cycles
η_{ch}/η_{dis}	0.95/0.95
SOC_{min}/SOC_{max}	0.10/0.90
α	50×10^4 CNY/MWh
β	18×10^4 CNY/MW
λ_{cur}	0.012×10^4 CNY/MWh
P_{min}/P_{max}	10–180 MW
E_{min}/E_{max}	20–720 MWh
ω	0.008
$SOC_s(24)/SOC_s(0)$	0.50/0.50
$\lambda_{lease,P}$	36×10^4 CNY/MW/year
$\lambda_{lease,E}$	12×10^4 CNY/MWh/year
$\lambda_{cap}^M/\lambda_{mil}^M$	$0.0010/0.00045 \times 10^4$ CNY/MWh
K_m/K_{perf}	6.0/0.88
K_{freq}/DOD_{ref}	4.5%/0.10

Note: The probability coefficient denotes the normalized seasonal sample proportion and is used as the annualization weight in the annual economic and cycling calculations. The difference coefficient denotes the normalized deviation between the selected representative day and the corresponding seasonal sample set; it is used only to evaluate the representativeness of the selected typical day.

(4) Power-to-Energy Capacity Ratio Constraint

The power-to-energy capacity ratio of shared energy storage should be maintained within a reasonable range to ensure sufficient charge–discharge rate capability and avoid excessive power configuration.

$$\frac{P}{E} \in [0.25, 1.0] \tag{18}$$

Equation (18) is used to limit the range of the power-to-energy capacity ratio of energy storage.

Through the above objective function and constraints, the upper-level model can comprehensively trade off revenue improvement, lifetime degradation, and investment boundaries, and dynamically correct the configuration results using the annual equivalent number of cycles fed back from the lower level.

3.5. Lower-Level Day-Ahead Dispatch Model

3.5.1. Lower-Level Objective Function

Given P, E, and the service-reservation boundaries, the lower-level model first maximizes spot-market arbitrage revenue. To avoid non-unique curtailed-energy results when the arbitrage revenues are identical or approximately identical, a small-weight curtailed-energy minimization term is further introduced to stably select a dispatch solution that also considers curtailed-energy accommodation:

$$max\ \pi_{day,s} = \sum\nolimits_{t=1}^{24} \pi_s(t)\left[P_{dis,s}^{arbi}(t) - P_{ch,s}^{arbi}(t)\right]\Delta t - \varepsilon\sum\nolimits_{t=1}^{24} P_{cur,s}(t)\Delta t \tag{19}$$

where $\pi_{day,s}$ denotes the objective function value of the lower-level dispatch problem for representative day s; $P_{dis,s}^{arbi}(t)$ and $P_{ch,s}^{arbi}(t)$ denote the discharging and charging power for spot-market arbitrage, respectively; $P_{cur,s}(t)$ denotes the actual curtailed power; ε denotes a sufficiently small positive number. In this paper, ε is set to $10^{-6} \times 10^4$ CNY/MWh, which is much smaller than the nonzero price spread of a representative day. It is used only to preferentially select the dispatch scheme with lower curtailed energy when the spot-market arbitrage revenues are identical or approximately identical and is not regarded as the actual curtailed-energy penalty cost in the upper-level annualized economic evaluation.

3.5.2. Lower-Level Constraints and Power Decomposition Logic

The lower-level power-capacity space consists of leasing reserves, frequency-regulation reserves, and market-based arbitrage space. Leasing reserves are first used to satisfy reliability-support dispatch, and their idle part is used for passive accommodation of curtailed renewable energy. Market-based arbitrage only uses the remaining power space after deducting the leasing reserve power and frequency-regulation reserve power.

(1) Power Balance Constraint

$$\begin{cases} P_{re,s}(t) + P_{dis,s}(t) - P_{ch,s}(t) - P_{cur,s}(t) = P_{grid,s}(t) \\ 0 \le P_{grid,s}(t) \le P_{grid,s}^{lim}(t) \\ 0 \le P_{cur,s}(t) \le P_{cur,s}^{max}(t) \\ P_{cur,s}^{max}(t) = max\left\{0, P_{re,s}(t) - P_{grid,s}^{lim}(t)\right\} \end{cases} \tag{20}$$

where $P_{ch,s}(t)$ and $P_{dis,s}(t)$ denote the total physical charging and discharging power of the energy storage system in time period t of representative day s, respectively; $P_{grid,s}(t)$ denotes the auxiliary variable of actual grid-connected power determined by the power balance constraint; $P_{re,s}(t)$ denotes the renewable energy output; and $P_{grid,s}^{lim}(t)$ denotes the exogenously specified upper limit of grid-connected power. Since both $P_{re,s}(t)$ and $P_{grid,s}^{lim}(t)$ are exogenous inputs, $P_{cur,s}^{max}(t)$ is pre-calculated before the lower-level optimization. Therefore, the max operation in Equation (20) does not introduce a new nonlinear decision relationship. This equation constrains the actual curtailed power not to exceed the upper limit of potential curtailed power in the corresponding time period. When the renewable energy output is higher than the grid-connected power limit, the excess part forms potential curtailment; otherwise, the potential curtailed power is zero.

(2) Total Power Decomposition Constraint

$$
\begin{cases}
P_{ch,s}(t) = P_{ch,s}^{arbi}(t) + P_{ch,s}^{abs}(t) \\
P_{dis,s}(t) = P_{dis,s}^{arbi}(t) + P_{dis,s}^{lease}(t) \\
0 \le P_{ch,s}^{abs}(t) \le P_{cur,s}^{max}(t)
\end{cases} \tag{21}
$$

where $P_{ch,s}^{abs}(t)$ denotes the charging power for passive accommodation of curtailed renewable energy undertaken by idle leased reserve resources; $P_{dis,s}^{lease}(t)$ denotes the discharging power generated by leased reserve resources during reliability-support dispatch; and $P_{cur,s}^{max}(t)$ denotes the upper limit of curtailed power that can be accommodated in time period t of representative day s, whose value is determined by Equation (20).

(3) Converter Power Boundary Constraint

Considering the priority occupation of leased resources by reliability-support services for renewable energy stations, let $P_{call,s}(t)$ denote the exogenously specified reliability-support dispatch power in time period t of representative day s, satisfying $0 \le P_{call,s}(t) \le P_{lease}$. In this study, $P_{call,s}(t)$ is constructed as a prescribed engineering reliability-support scenario rather than an additional decision variable of the lower-level model. It represents the reserve call of renewable energy stations under reliability-support requirements. Before being introduced into the lower-level dispatch model, this profile is checked against the leased reserve power, the SOC upper and lower limits, and the initial-terminal SOC closure condition. Therefore, the lower-level model optimizes passive accommodation and spot-market arbitrage only under reliability-support profiles that are already feasible in terms of power and energy. This paper assumes that the exogenous reliability-support dispatch power $P_{call,s}(t)$ already satisfies the power and SOC feasibility requirements of the energy storage system. The leased reserve resources should first meet the reliability-support dispatch demand, namely $P_{dis,s}^{lease}(t) = P_{call,s}(t)$. The uncalled leased reserve power, $P_{lease} - P_{call,s}(t)$, can be used for passive accommodation of curtailed renewable energy during idle periods. Based on the operating principle of "reserve priority, idle-space accommodation, and residual market-based dispatch", spot-market arbitrage only uses the dedicated adjustable space after deducting the leased reserve power and frequency-regulation reserve power. Idle leased resources do not participate in active arbitrage and are used only for passive accommodation of curtailed renewable energy.

$$
\begin{cases}
0 \le P_{ch,s}^{arbi}(t) \le U_{ch,s}(t) \cdot \left(P - P_{lease} - P_{freq}\right) \\
0 \le P_{dis,s}^{arbi}(t) \le U_{dis,s}(t) \cdot \left(P - P_{lease} - P_{freq}\right) \\
0 \le P_{ch,s}^{abs}(t) \le U_{ch,s}(t) \cdot (P_{lease} - P_{call,s}(t)) \\
P_{dis,s}^{lease}(t) = P_{call,s}(t) \\
P_{dis,s}^{lease}(t) \le U_{dis,s}(t) \cdot P_{lease} \\
0 \le P_{call,s}(t) \le P_{lease} \\
P_{lease} + P_{freq} \le P \\
U_{ch,s}(t) + U_{dis,s}(t) \le 1 \\
U_{ch,s}(t), U_{dis,s}(t) \in \{0,1\}
\end{cases} \tag{22}
$$

where $P_{call,s}(t)$ denotes the exogenously specified reliability-support dispatch power; P_{lease} denotes the leased reserve power; P_{freq} denotes the frequency-regulation reserve power; P denotes the rated power of shared energy storage; and $U_{ch,s}(t)$ and $U_{dis,s}(t)$ denote the charging status variable and discharging status variable of energy storage in time period t of representative day s, respectively.

(4) SOC Dynamics and Boundary Constraints

$$\begin{cases} SOC_s(t) = SOC_s(t-1) + \frac{\left(P_{ch,s}(t)\cdot\eta_{ch} - P_{dis,s}(t)/\eta_{dis}\right)\Delta t}{E} \\ SOC_{min} \le SOC_s(t) \le SOC_{max} \\ SOC_s(24) = SOC_s(0) = SOC_0 \end{cases} \tag{23}$$

where $SOC_s(t)$ denotes the state of charge of the energy storage system at the end of time period t on representative day s; $SOC_s(t-1)$ denotes the state of charge at the end of time period $t-1$; In Equation (23), SOC_0 denotes the initial SOC of the representative day, which is set to $SOC_0 = 0.50$ in this paper. The constraint $SOC_s(24) = SOC_s(0)$ represents the initial–terminal SOC closure of the representative day, which is used to prevent the model from obtaining unrealistic discharging revenue by overdrawing the terminal SOC [33].

(5) Hard Constraint on the Curtailment Rate

$$\sum_{t=1}^{24} P_{cur,s}(t)\cdot\Delta t \le \gamma\cdot\sum_{t=1}^{24} P_{re,s}(t)\cdot\Delta t \tag{24}$$

where γ denotes the maximum curtailment rate allowed by the power grid, and this constraint holds separately for each representative day.

3.6. Feedback Variable Calculation and Closed-Loop Interface

After the lower-level optimization is completed, the optimal dispatch solution y_s^* is first obtained from Equation (19). Then, $\pi_{spot,s}^*$ is calculated according to the definition of net spot-market arbitrage revenue in Equation (11), and R_{spot} is obtained through annualization. The curtailed energy of the representative day is calculated as follows:

$$E_{cur,s}^* = \sum_{t=1}^{24} P_{cur,s}(t)\cdot\Delta t \tag{25}$$

where $E_{cur,s}^*$ denotes the total curtailed energy of representative day s, with the unit of MWh/day. It should be noted that $E_{cur,s}^*$ is substituted into Equation (14) of the upper-level model, and the annualized curtailed-energy penalty cost C_{cur} is calculated in combination with the representative-day weights. To avoid double counting, the actual curtailed-energy penalty cost is not directly deducted in the lower-level objective function. Only the sufficiently small weight ε is retained for tie-breaking among equivalent optimal solutions. The actual annualized curtailed-energy penalty cost is uniformly calculated at the upper level based on the feedback curtailed energy.

The annual equivalent number of cycles is calculated using the service-mode-specific cycle calculation method described in Section 3.1. Specifically, the arbitrage discharging power is substituted into Equations (1) and (3) to obtain N_{arbi}; leasing-related testing, maintenance, reliability-support dispatch, and passive accommodation form N_{lease}; frequency-regulation response power forms N_{freq}; and N_{real} is obtained from Equation (5). Among these feedback variables, $\pi_{spot,s}^*$, $E_{cur,s}^*$, and the dispatch results used for cycle conversion are used to calculate R_{spot}, C_{cur}, and N_{real}, respectively, and further update L_{real} and $C_{dep,real}$. Accordingly, the annualized net income F of a candidate capacity configuration can simultaneously reflect the lower-level dispatch revenue, curtailed-energy cost, and lifetime-depreciation variation caused by operational intensity.

4. Case Study Setup and Verification of the Dynamic Depreciation Model

To verify the proposed shared energy storage capacity configuration model and the dynamic depreciation closed-loop mechanism, a case study is conducted using representative-day data from a renewable energy base. This section presents the data sources and parameter settings, and then verifies the model through depreciation comparison, business-scheme comparison, representative-day operation analysis, and market-parameter sensitivity analysis.

4.1. Data Sources and Parameter Settings

The case study uses data from a renewable energy base consisting of two wind farms and two photovoltaic power stations. The dispatch horizon is 24 h with a time resolution of 1 h, and the total installed capacity is 384 MW. Seasonal representative days are selected based on typicality indicators and converted into annualization weights according to the number of seasonal samples. The grid-connected power limit of each representative day is set as an exogenous boundary to characterize transmission constraints and potential curtailment risk, while the spot electricity price adopts a unified 24-point time-of-use sequence. Shared energy storage is located on the renewable energy base side and provides leasing-based reliability support, passive accommodation of curtailed renewable energy, spot-market arbitrage, and frequency-regulation ancillary services [34]. Its charging energy mainly comes from available renewable energy and curtailed-energy accommodation on the renewable energy side, without considering reverse charging from the external grid. The typicality evaluation results are provided in Table A1.

To improve the transparency of the representative-day construction, the selection procedure is further described as follows. The case study covers the full year of 2020 with an hourly resolution. The annual samples are first divided into four seasonal subsets, namely spring, summer, autumn, and winter. For each seasonal subset, candidate days are evaluated according to typicality indicators that reflect the renewable-output profile, the occurrence of grid-connection constraints, and the potential curtailed-energy risk. The day with the best overall representativeness is then selected as the representative day for the corresponding season. The probability coefficient in Table A1 denotes the normalized proportion of annual samples represented by each seasonal subset and is used as the annualization weight. The difference coefficient measures the normalized deviation between the selected representative day and the corresponding seasonal sample set. It is used to evaluate the representativeness of the selected day, rather than as an annualization weight. Therefore, the representative-day dispatch results are converted into annual values using the probability coefficients, while the difference coefficients are reported only to indicate the typicality of the selected scenarios.

To improve the reproducibility of the main case-study results, a simplified representative-day reproducibility dataset is provided as Supplementary Materials. This dataset includes the 24 h representative-day renewable-output profiles for spring, summer, autumn, and winter, the hourly grid-connection limits, the potential curtailed-energy profiles, the hourly spot-market price series, and the main parameter tables used in the optimization. The representative-day profiles are the direct inputs to the lower-level MILP dispatch model, while the economic parameters, engineering boundaries, and business-scheme settings are used in the upper-level capacity configuration and annualized economic evaluation.

The upper bounds of power and energy capacity in Table 1 are engineering planning boundaries rather than unconstrained optimization results. In the benchmark case, $P_{max} = 180$ MW is determined by the grid-access capability, converter-capacity planning, and station-side installation feasibility of the renewable energy base. The corresponding upper energy-capacity bound $E_{max} = 720$ MWh represents the maximum planned energy-storage scale under the benchmark engineering setting. Therefore, the optimized capacity results should be interpreted as optimal configurations under the specified access, investment, market, and engineering-boundary conditions.

To unify the economic evaluation criteria, the initial investment of shared energy storage is calculated as $\mathrm{I}_0 = \alpha\mathrm{E} + \beta\mathrm{P}$. Since the annualized net income F has already deducted the capacity-side annualized depreciation cost and the power-side annualized investment cost, the operating net cash flow is reconstructed as $CF = F + C_{dep,eval} + C_P^{ann}$, where $C_{dep,eval}$ denotes the capacity-side annualized depreciation cost adopted in the evaluation model and C_P^{ann} denotes the power-side annualized investment cost. In the static depreciation model, $C_{dep,eval}$ is calculated using the fixed calendar life, whereas in the dynamic depreciation model it is taken as $C_{dep,real}$. These two annualized capital-cost terms are added back because they are accounting annualization items rather than actual annual operating cash outflows. The internal rate of return (IRR) is calculated by setting the net present value to zero, and the static payback period is calculated as $T_{PB} = I_0/CF$. In the static depreciation model, the evaluation period is the calendar life; in the dynamic depreciation evaluation, it is the actual economic lifetime.

As shown in Table 1, the reference cycle life is 6000 cycles, and the calendar life is 15 years, corresponding to a lifetime transition threshold of 400 cycles/year. In subsequent schemes, P is close to 180 MW, and E reaches or approaches the upper limit, indicating that the optimized results are affected by the engineering configuration boundaries.

Figure 3 presents the 24 h electricity price curve. The peak-valley spread provides the price signal for spot-market arbitrage and the incentive for releasing SOC space at different times.

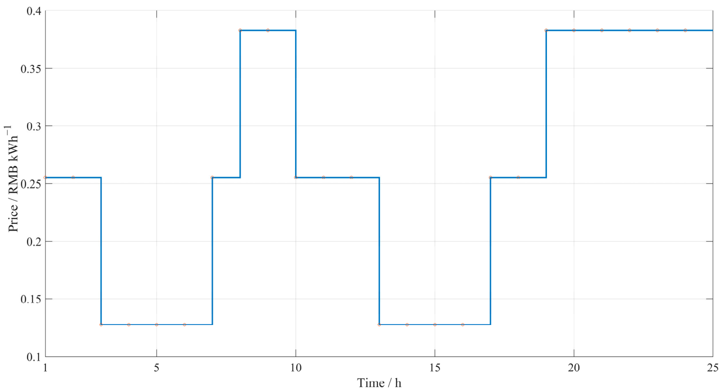

Figure 3. Representative-day electricity price profile. The circular markers indicate hourly price-sampling points.

Figure 4 shows that renewable output exceeds the grid-connected power limit during some periods of all seasonal representative days, indicating the existence of curtailed-energy accommodation demand. The representative-day weights are provided in Table A1.

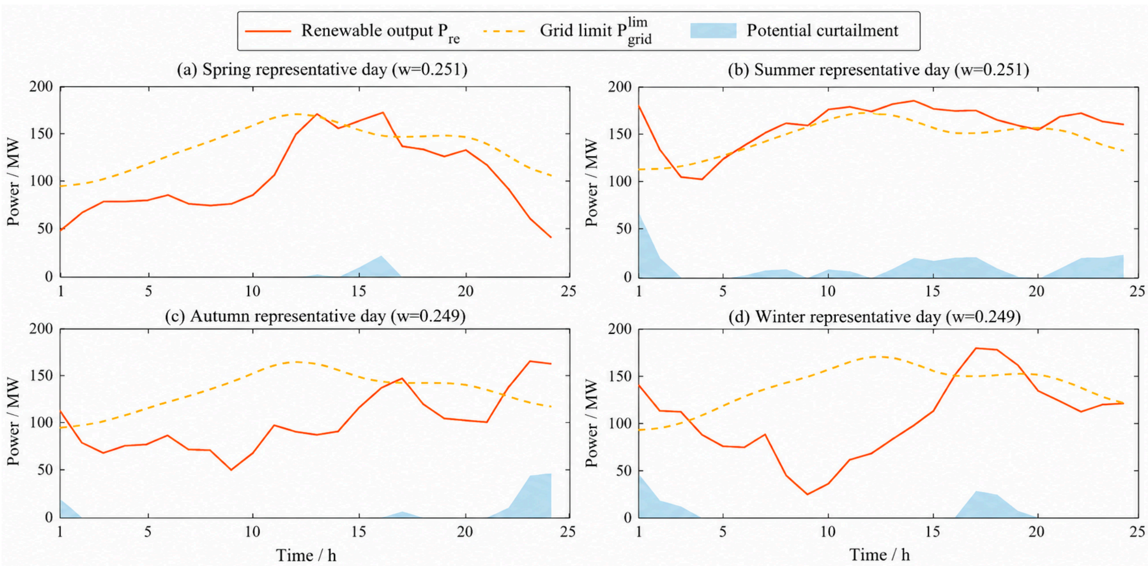

Figure 4. Renewable energy output and grid-connected power limits of seasonal representative days.

4.2. Effectiveness Verification of the Dynamic Depreciation-Based Capacity Configuration Model

To examine the effect of dynamic depreciation, three depreciation treatments are compared under the S2 service boundary. M1 is the static depreciation model with a fixed 15-year battery lifetime. M2 keeps the M1 configuration unchanged but evaluates the actual lifetime and dynamic depreciation cost using annual equivalent cycles. M3 is the proposed dynamic-depreciation closed-loop model, in which operational cycles are fed back into lifetime assessment and depreciation-cost calculation during capacity optimization.

Table 2 gives the numerical comparison, while Figure 5 visualizes the relative differences among M1, M2, and M3.

Table 2. Configuration, lifetime, and economic results under different depreciation models.

Model	P*/MW	E*/MWh	N_{real}/ (Cycles·Year^{-1})	Evaluated Lifetime/Year	Capacity-Side Depreciation Cost/ (10^4 CNY·Year^{-1})	Annualized Net Income/ (10^4 CNY·Year^{-1})	IRR/%	Payback Period/Year
M1	180	533	476.71	15.00	3113.51	4597.89	26.24	3.69
M2	180	533	476.71	12.59	3436.46	4274.93	25.68	3.69
M3	180	720	403.04	14.89	4222.89	4395.90	21.73	4.36

Note: M1 and M2 have the same payback period because they use the same capacity configuration and dispatch results; the difference between them lies in the evaluated economic lifetime and annualized depreciation cost rather than in the initial investment or operating cash-flow recovery process.

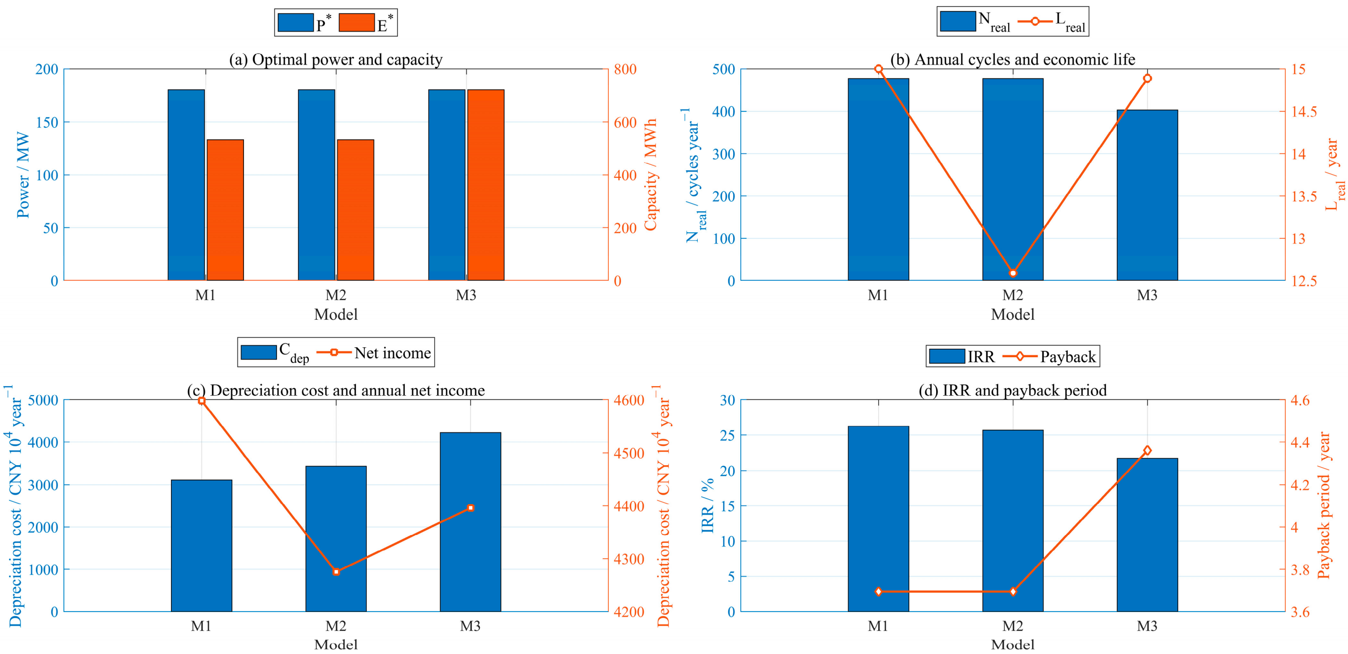

Figure 5. Comparison of configuration, lifetime, and economic indicators under M1, M2, and M3.

As shown in Table 2 and Figure 5, M1 selects E* = 533 MWh and produces 476.71 cycles/year, exceeding the 400 cycles/year lifetime-transition threshold. Under the same configuration, M2 reduces the evaluated lifetime to 12.59 years, increases the capacity-side depreciation cost to 3436.46 × 10^4 CNY/year, and decreases annualized net income to 4274.93 × 10^4 CNY/year. This indicates that static depreciation overestimates the economic performance of high-cycling schemes. Compared with M2, M3 expands E* to 720 MWh, reduces N_{real} to 403.04 cycles/year, restores the lifetime to 14.89 years, and increases annualized net income by 120.97 × 10^4 CNY/year. Although its IRR is lower and payback period is longer due to the larger initial investment, M3 better reflects the trade-off among capacity scale, cycling intensity, lifetime degradation, and annualized income. The boundary values of P* and E* also indicate that the result should be interpreted as an optimum under the given access, cost, price, and capacity limits.

Although M1 and M2 have different evaluated lifetimes and annualized net incomes, their payback periods are the same because M2 is an ex post dynamic-depreciation evaluation of the M1 capacity configuration. Therefore, M1 and M2 share the same P*/E* configuration, initial investment, and representative-day dispatch results. The payback period is calculated according to the recovery of the initial investment by operating cash flows, rather than by the accounting annualized depreciation cost. Consequently, the dynamic lifetime correction in M2 changes the annualized depreciation cost and annualized net income, but it does not change the cash-flow recovery process under the same configuration and dispatch.

Figure 6 explains the mechanism behind Table 2: once annual equivalent cycles exceed 400 cycles/year, economic lifetime declines and unit capacity-side dynamic depreciation cost increases, converting operational intensity into a cost signal for capacity configuration.

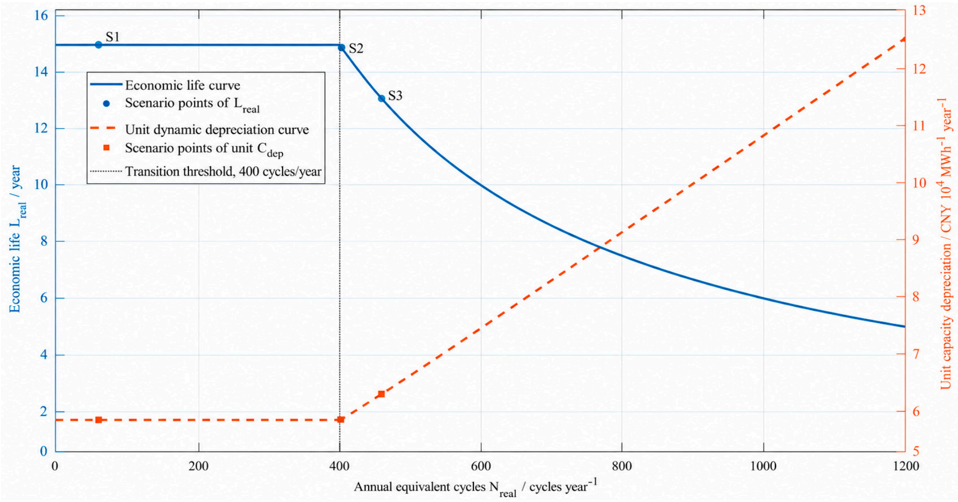

Figure 6. Relationship among annual equivalent cycles, economic lifetime, and unit capacity-side dynamic depreciation cost.

4.3. Economic Operation Analysis of Shared Energy Storage Under Different Business Schemes

Three business schemes are compared. S1 includes leasing-based reliability support and passive accommodation of curtailed renewable energy. S2 adds spot-market arbitrage to S1, while S3 further incorporates frequency-regulation ancillary services. For all schemes, the capacity configuration is re-optimized under the corresponding service boundaries, and the detailed settings are provided in Table A2. The parameter settings of S1, S2, and S3 are not intended to represent a purely additive revenue comparison with all boundary parameters fixed. Instead, they are designed to represent three feasible business-boundary scenarios under the priority principle of "reserve first, idle-space accommodation, and residual market-based dispatch". Specifically, S1 represents a leasing-dominated operation mode, in which a relatively larger proportion of power capacity is reserved for reliability support and only idle leased resources are used for passively curtailed-energy accommodation. S2 introduces spot-market arbitrage and therefore retains part of the converter capacity as arbitrage-available power after satisfying the leasing boundary. S3 further reserves part of the converter capacity for frequency-regulation services, which reduces the power space available for arbitrage and changes the cycling-intensity level. The corresponding leasing reserve ratios, frequency-regulation reserve ratio, and maintenance-cycle assumptions are reported in Table A3 and are used to define internally consistent service-boundary scenarios rather than isolated service additions.

Table 3 summarizes the cycling, lifetime, and net-income results; Figure 7 further presents the economic-performance comparison from three aspects, including revenue composition and annual net income, cost composition and total annual cost, and annual curtailment and curtailment penalty; Figure 8 separates the cycle sources.

Table 3. Cycling, lifetime, and economic results under different business schemes.

Scheme	N_{lease}/ (Cycles·Year^{-1})	N_{arbi}/ (Cycles·Year^{-1})	N_{freq}/ (Cycles·Year^{-1})	N_{real}/ (Cycles·Year^{-1})	L_{real}/Year	Annualized Net Income/ (10^4 CNY·Year^{-1})
S1	59.70	0.00	0.00	59.70	15.00	1188.98
S2	87.35	315.69	0.00	403.04	14.89	4395.90
S3	108.99	336.55	13.54	459.08	13.07	3751.81

Note: The service-boundary parameters of S1, S2, and S3 are scenario settings used to represent different feasible business modes. They are not designed as a single-factor experiment in which only one service is added while all other boundary parameters remain unchanged. Therefore, the economic differences among S1, S2, and S3 reflect the combined effects of service participation, reserve-capacity occupation, arbitrage-space availability, maintenance-cycle assumptions, and dynamic-depreciation feedback.

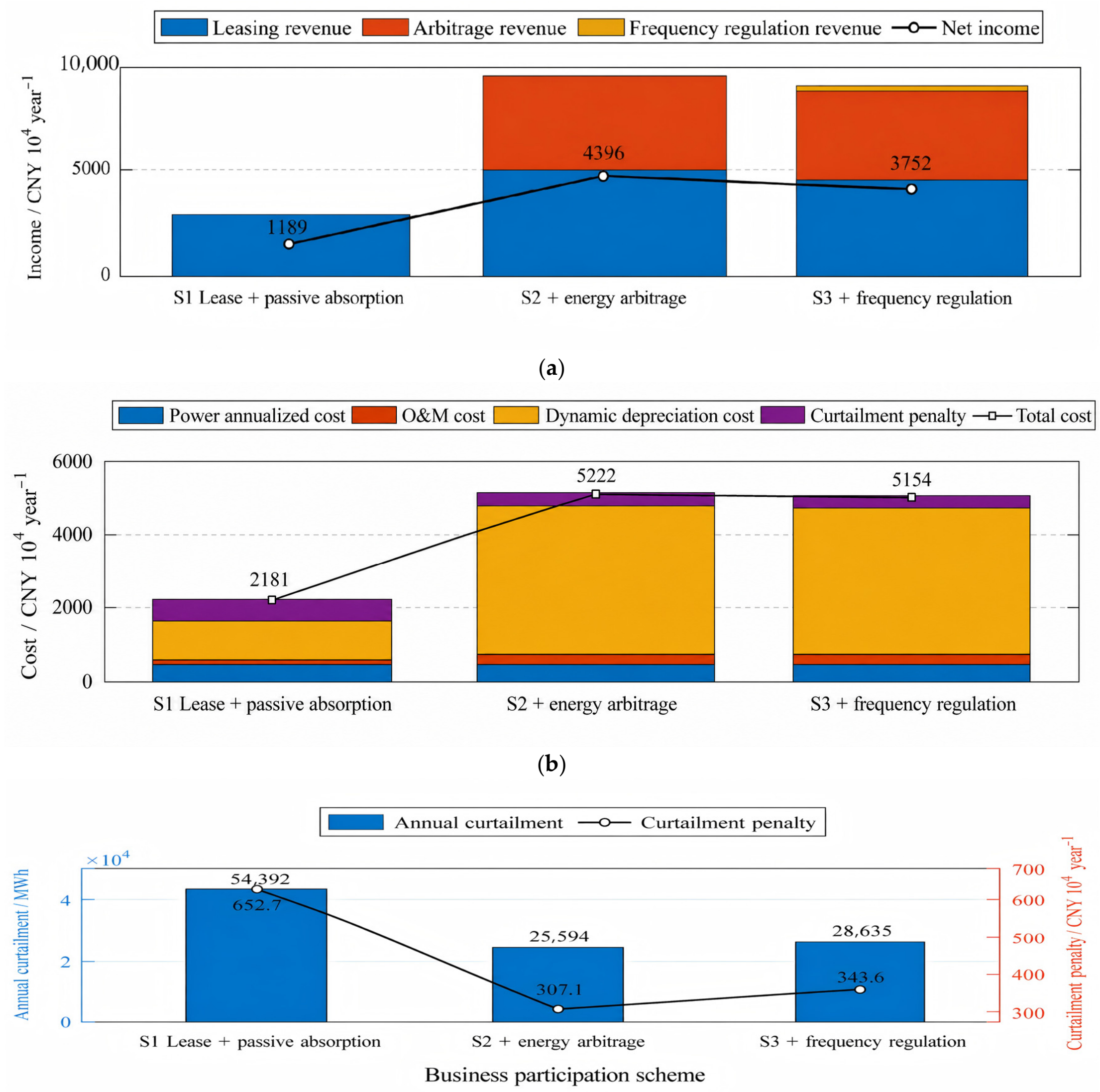

(a) (b) (c)

Figure 7. Economic-performance comparison under different business participation schemes: (**a**) revenue composition and annual net income; (**b**) cost composition and total annual cost; (**c**) annual curtailment and curtailment penalty.

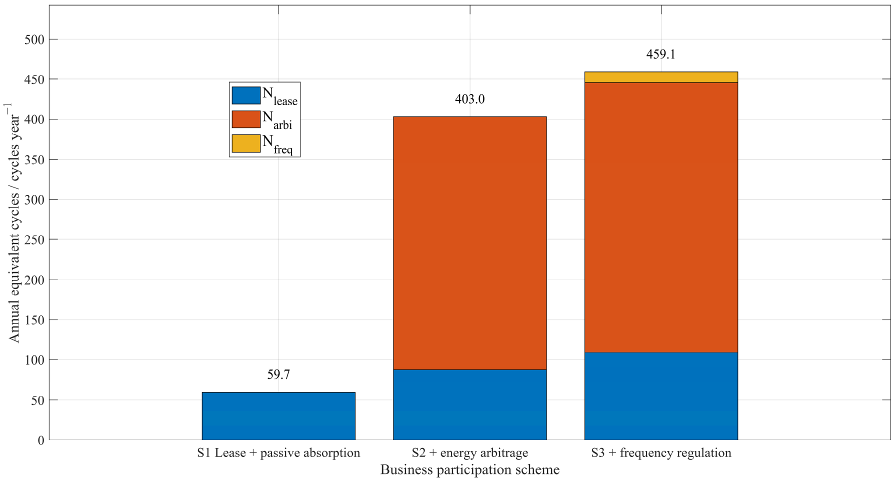

Figure 8. Composition of annual equivalent cycle sources under different business schemes.

As shown in Table 3 and Figure 7a, S1 obtains 1188.98 $\times$ 10^4 CNY/year of annualized net income with only 59.70 cycles/year. After spot-market arbitrage is introduced in S2, N_{arbi} increases to 315.69 cycles/year, and the annualized net income rises to 4395.90 $\times$ 10^4 CNY/year. Figure 7b shows that the total annual cost also increases because the larger optimized capacity and higher multi-service cycling intensity raise the dynamic depreciation cost. Figure 7c further shows that annual curtailment decreases from 54,392 MWh in S1 to 25,594 MWh in S2, indicating that the combination of passive accommodation and spot-market arbitrage improves SOC-space utilization and curtailed-energy accommodation. Although S3 gains frequency-regulation revenue, frequency-regulation reserves occupy part of the adjustable power capacity and increase N_{real} to 459.08 cycles/year, reducing L_{real} to 13.07 years and making its annualized net income lower than that of S2 under the benchmark compensation level. Therefore, S2 is selected as the preferred scheme under the benchmark conditions.

It should be emphasized that the comparison among S1, S2, and S3 reflects the combined effects of service addition and service-boundary settings. The increase in annualized net income from S1 to S2 is mainly related to the introduction of spot-market arbitrage and the improved use of SOC space for passive accommodation. However, it is also affected by the adjusted leasing boundary and maintenance-cycle assumptions. Similarly, the lower annualized net income of S3 under the benchmark compensation level is not caused by frequency-regulation participation alone, but by the combined effect of frequency-regulation revenue, reserve-capacity occupation, reduced arbitrage-available power, increased cycling intensity, and higher dynamic depreciation pressure.

Figure 8 further shows that the increase in S2 mainly comes from price-driven arbitrage cycles, whereas the additional cycles in S3 include the frequency-regulation component. This supports the conclusion that scheme selection should consider both revenue increments and dynamic depreciation costs.

4.4. Verification of Representative-Day Dispatch Strategy and Operating Mechanism

To explain the operating mechanisms of different business schemes, the spring representative day of 26 April 2020 is selected to analyze power allocation, SOC variation, and curtailed-energy accommodation. These results illustrate representative-day operation, while annualized economic performance is still evaluated using the weighted results of four seasonal representative days.

Figures 9 and 10 describe the dispatch process from external power balance and internal storage allocation, respectively; Table 4 then summarizes the corresponding accommodation and arbitrage statistics. The corresponding SOC trajectories under different business schemes are provided in Figure A1.

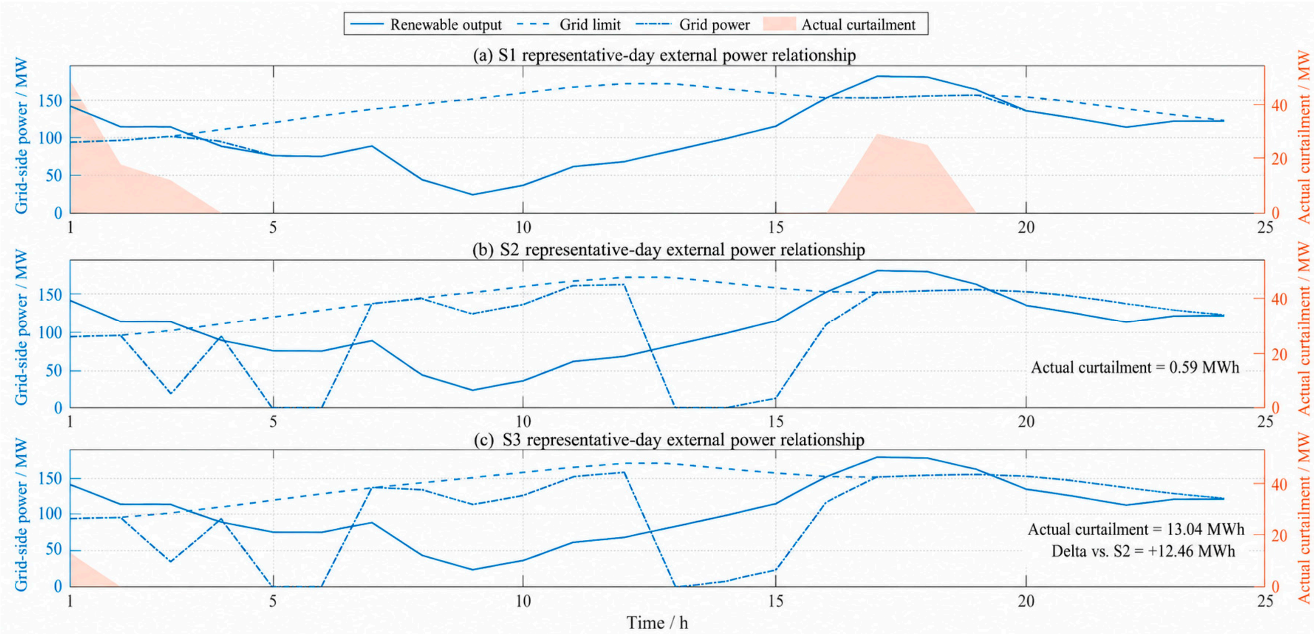

Figure 9. External power relationships of S1, S2, and S3 on the representative day.

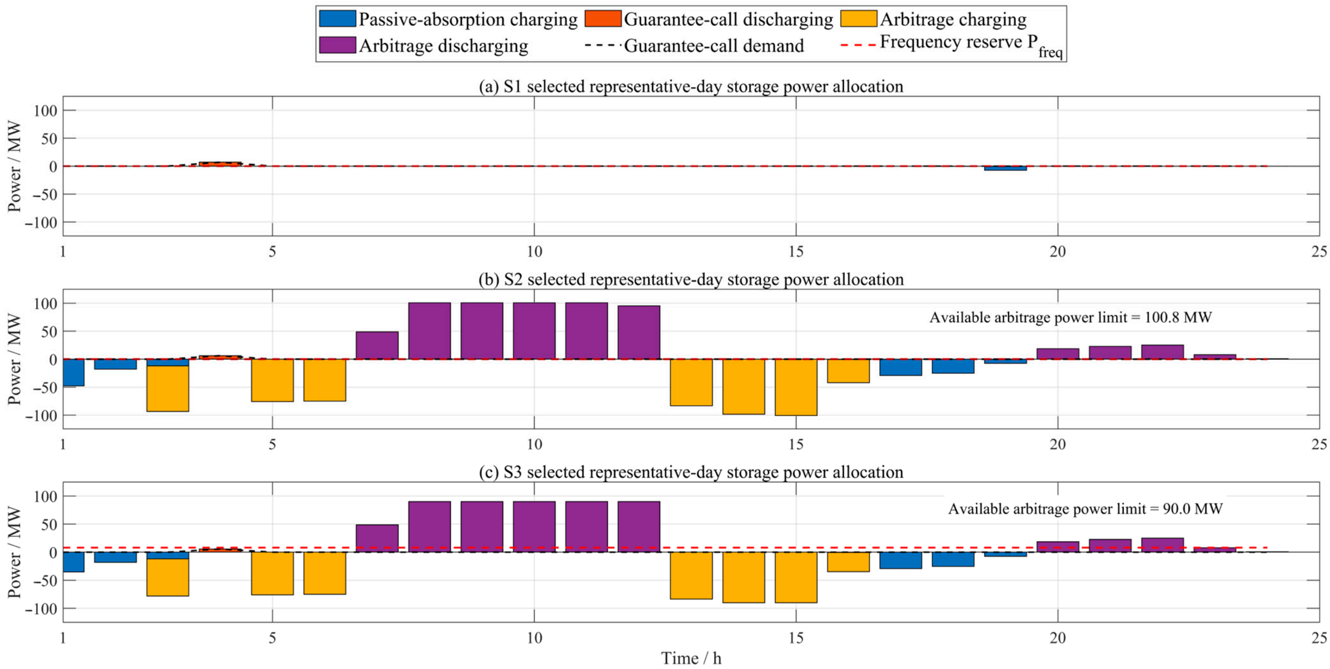

Figure 10. Energy storage power allocation of S1, S2, and S3 on the representative day.

Table 4. Representative-day curtailed-energy accommodation and arbitrage dispatch results.

Scheme	Potential Curtailed Energy/MWh	Passive Accommodation/MWh	Actual Curtailed Energy/MWh	Arbitrage Charging Energy/MWh	Arbitrage Discharging Energy/MWh
S1	140.44	7.78	132.66	0.00	0.00
S2	140.44	139.86	0.59	556.65	622.35
S3	140.44	127.40	13.04	514.75	573.92

Figure 9 shows the external relationship among renewable output, grid-connection limits, curtailed energy, and grid-connected power.

Figure 10 decomposes the internal power allocation of shared energy storage under the three schemes, explaining the operational source of the differences observed in Figure 9.

As shown in Figures 9 and 10 and Table 4, the actual curtailed energy in S1 is 132.66 MWh. In S2, arbitrage discharging releases SOC space, increasing passive accommodation to 139.86 MWh and reducing actual curtailment to 0.59 MWh. In S3, frequency-regulation reserves reduce the available dispatch space, decreasing passive accommodation to 127.40 MWh and increasing actual curtailment to 13.04 MWh. The arbitrage charging and discharging values in Table 4 are statistical results of the arbitrage power channel and do not form an independent energy-closure relationship; the overall energy balance is governed by the SOC dynamic equation and the initial-terminal SOC closure constraint in Equation (23).

The charging and discharging quantities reported in Table 4 are channel-specific statistical quantities used for revenue calculation and cycle attribution. They do not imply that each service channel must be independently energy balanced. The physical energy balance of the shared energy storage system is enforced at the system level by the SOC dynamic constraint, SOC upper and lower limits, and the initial-terminal SOC closure condition. As shown by the SOC trajectories in Figure A1, the SOC remains within the allowable range and returns to the specified terminal level for each representative day. Therefore, the channel-specific statistics in Table 4 should be interpreted together with the SOC trajectories in Figure A1.

4.5. Verification of Key Mechanisms and Sensitivity Analysis

4.5.1. Verification of the Passive Curtailed-Energy Accommodation Mechanism

To verify the role of passive curtailed-energy accommodation, S2 is used as the benchmark, the passive accommodation function is disabled, and the capacity configuration is then re-optimized. As shown in Figure 11, disabling passive accommodation increases annual curtailed energy from 25,594.30 MWh to 56,744.74 MWh and decreases annualized net income from 4395.90 $\times$ 10^4 CNY to 3108.88 $\times$ 10^4 CNY. Therefore, passive accommodation improves economic performance by reducing curtailment penalties and utilizing idle leased resources, and its cycling contribution should be attributed to leasing-related cycles rather than spot-market arbitrage cycles [35].

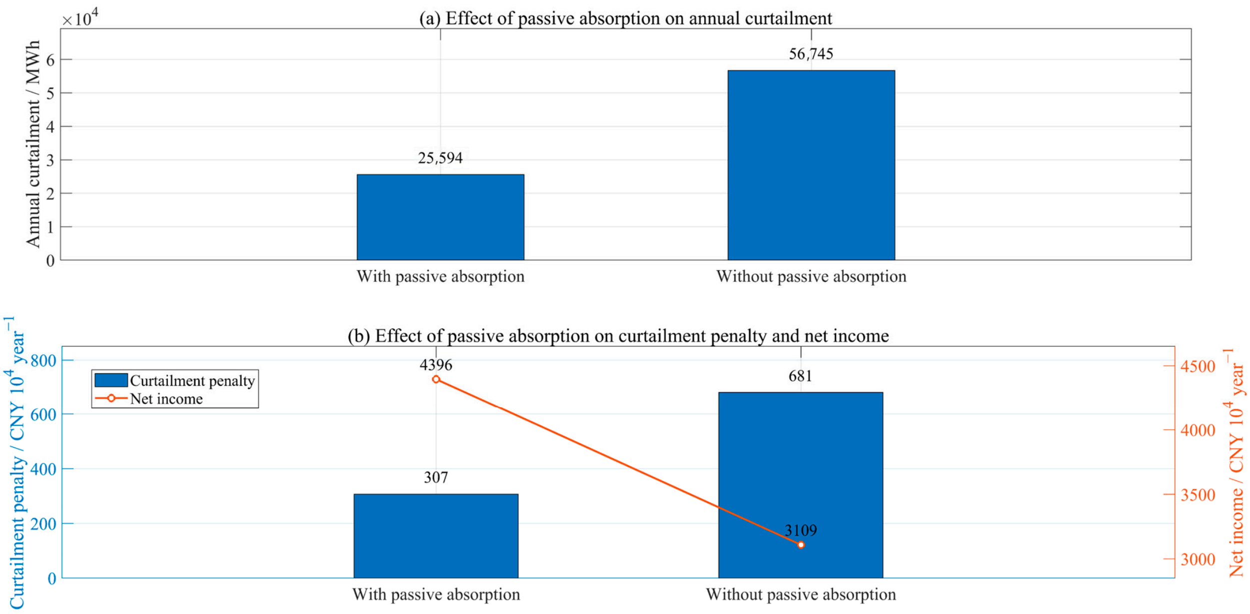

Figure 11. Ablation analysis of the passive curtailed-energy accommodation mechanism.

4.5.2. Market Parameter Sensitivity and Preferred Business Scheme

To examine parameter robustness, sensitivity analyses are conducted on electricity price scaling, unit leasing prices, and frequency-regulation compensation. The proposed depreciation mechanism should be interpreted as an economic planning model based on annual equivalent cycles, rather than as a full electrochemical battery degradation model, and curtailed-energy penalty. The electricity price scaling results are reported in Table 5 and Figure A2, while the sensitivity results for unit leasing prices, frequency-regulation compensation, and curtailed-energy penalty are shown in Figure 12 and Table 5.

Table 5. Market parameter sensitivity analysis results.

Sensitivity Parameter	Low Value	High Value	Annualized Net Income at Low Value/ (10^4 CNY·Year^{-1})	Annualized Net Income at High Value/ (10^4 CNY·Year^{-1})	Result at Low Value	Result at High Value
Electricity price scaling factor	0.65	1.40	2791	6274	P*/E* = 180/707 MW/MWh	P*/E* = 180/720 MW/MWh
Leasing price multiplier	0.50	2.00	2152	9364	S2	S2
Frequency-regulation compensation multiplier	0.50	5.00	4396	4708	S2	S3
Curtailed-energy penalty multiplier	0.50	2.00	4549	4089	S2	S2

Note: For the electricity price scaling factor, the result denotes P*/E*; for the other parameters, it denotes the preferred business scheme.

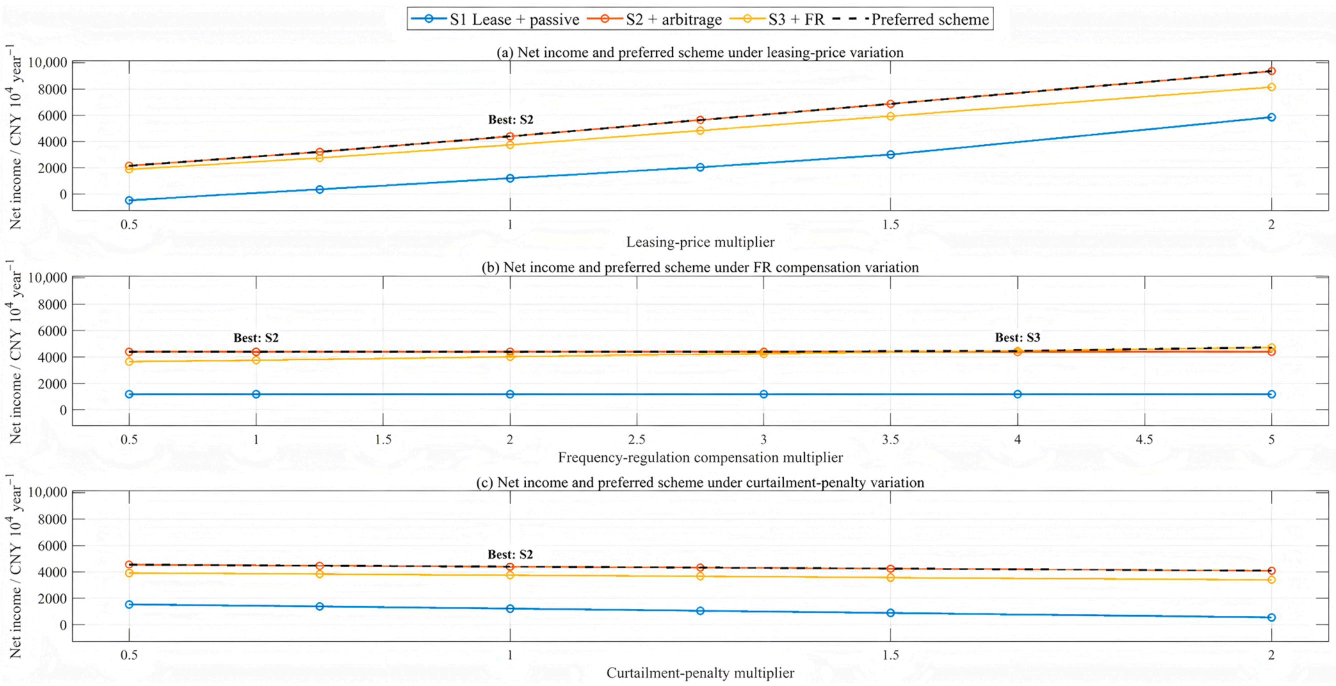

Figure 12. Sensitivity of unit leasing price, frequency-regulation compensation, and curtailed-energy penalty, and the preferred business scheme.

Figure 12 shows the sensitivity trends, and Table 5 provides the corresponding low- and high-value endpoint results.

As shown in Figure 12 and Table 5, increasing the electricity price scaling factor from 0.65 to 1.40 raises annualized net income from 2791 $\times$ 10^4 CNY/year to

6274×10^4 CNY/year and increases the optimal energy capacity from 707 MWh to 720 MWh, indicating that electricity price mainly affects arbitrage revenue and boundary utilization. Under variations in unit leasing prices and curtailed-energy penalty, S2 remains preferred.

To further identify the economic switching point between S2 and S3, a refined sweep of the frequency-regulation compensation multiplier was conducted around the transition region. As shown in Table A6, S2 remains preferable when $K_{FR} \leq 3.65$,whereas S3 becomes preferable from $K_{FR} = 3.70$ under the adopted 0.05 scanning resolution. Linear interpolation between $K_{FR} = 3.65$ and $K_{FR} = 3.70$ gives an estimated switching threshold of $K_{FR} \approx 3.6815$. Therefore, under the benchmark service-boundary and dynamic-depreciation assumptions, S3 becomes economically preferable only when the frequency-regulation compensation level increases to approximately 3.68 times the benchmark value. Below this threshold, the additional frequency-regulation revenue cannot offset reserve-capacity occupation, reduced arbitrage-available power, increased cycling intensity, and higher dynamic depreciation pressure.

4.5.3. Capacity-Boundary Sensitivity Analysis

In the benchmark M3 and S2 results, the optimized energy capacity reaches the imposed upper bound of 720 MWh. To further examine whether this result is mainly restricted by the upper energy-capacity boundary, an additional sensitivity test is conducted by expanding E_{max} from 720 MWh to 840 MWh and 960 MWh, while keeping the power-capacity upper bound, market parameters, grid-connection constraints, and service-boundary settings unchanged. Since the model also imposes an upper limit on the E/P ratio, the E/P upper bound is relaxed consistently with the expanded E_{max} to avoid retaining the original 4 h duration boundary.

As shown in Table 6, when E_{max} is increased from 720 MWh to 840 MWh, the optimized energy capacity increases only slightly from 720 MWh to 728 MWh, and the annualized net income increases from 4395.90×10^4 CNY/year to 4400.79×10^4 CNY/year, corresponding to an increase of approximately 0.11%. When E_{max} is further increased to 960 MWh, the optimized configuration and annualized net income remain unchanged. These results indicate that the benchmark solution is affected by the imposed energy-capacity boundary, but the marginal economic benefit of further expanding the energy capacity is very limited. Therefore, the benchmark M3 result should be interpreted as a boundary-conditioned optimum close to the economic saturation region under the given market, grid-connection, service-boundary, and dynamic-depreciation assumptions. It should also be noted that the optimized power capacity remains at the upper bound of 180 MW, indicating that the result is still conditioned by the engineering power-access boundary.

Table 6. Sensitivity of the optimized M3 configuration to the upper energy-capacity bound.

E_{max}/MWh	E/P Upper /h	P*/MW	E*/MWh	N_{real}/ (Cycles·Year^{-1})	L_{real}/Year	Annualized Net Income/ (10^4 CNY·Year^{-1})
720	4.00	180	720	403.04	14.89	4395.90
840	4.67	180	728	400.18	14.99	4400.79
960	5.33	180	728	400.18	14.99	4400.79

4.6. Applicability and Limitations of the Proposed Model

The proposed model is most applicable to renewable energy bases where shared energy storage simultaneously provides leasing-based reliability support, passive curtailed-energy accommodation, spot-market arbitrage, and frequency-regulation reserve under clearly defined service boundaries. The representative-day reduction is appropriate when the selected seasonal profiles can adequately capture renewable-output patterns, grid-connection constraints, and curtailed-energy risk characteristics of the annual samples. Under these conditions, the model can evaluate how service-boundary allocation and cycling intensity affect capacity configuration, economic lifetime, dynamic depreciation cost, and annualized net income.

The model may become less reliable when actual operation deviates from the benchmark assumptions. First, if extreme renewable-output events or grid-connection restrictions are not represented by the selected typical days, the annual revenue, curtailed-energy reduction, and cycling-intensity evaluation may be biased. Second, if market rules or contractual arrangements allow the service boundaries to be dynamically redefined, for example, if passive accommodation becomes an independently priced service or frequency-regulation reserve is co-optimized with energy arbitrage at a higher time resolution, the boundary parameters should be recalibrated. Third, the current frequency-regulation treatment assumes an approximately zero-mean response at the day-ahead dispatch timescale; persistent regulation-energy bias or high-resolution regulation trajectories with nonzero cumulative energy should be explicitly incorporated into the SOC dynamics. Fourth, the dynamic depreciation mechanism is a planning-level economic depreciation model based on annual equivalent cycles. It does not explicitly capture temperature dependence, C-rate effects, variable depth-of-discharge ageing, SOC-dependent calendar ageing, or state-of-health-dependent capacity fade. Therefore, applications requiring detailed battery-health prediction should replace or extend the equivalent-cycle-based lifetime function with a more detailed degradation model. Finally, the optimized capacity and preferred business scheme remain conditional on market prices, compensation levels, grid-connection limits, and configuration boundaries. Cross-regional applications should therefore recalibrate these parameters and, when necessary, repeat the market-parameter and capacity-boundary sensitivity analyses.

5. Conclusions

Based on representative-day data from a renewable energy base, this paper verifies the shared energy storage capacity configuration model, the dynamic-depreciation closed-loop mechanism, and the multi-service operation strategy through a case study. The main conclusions are as follows.

(1) The dynamic-depreciation closed-loop mechanism can correct the overestimation of the economic performance of high-cycling schemes caused by static depreciation. The ex post dynamic evaluation in M2 shows that, for the M1 configuration, the actual economic lifetime decreases to 12.59 years and the annualized net income decreases to 4274.93×10^4 CNY. Through cycle feedback, M3 increases the energy capacity from 533 MWh to 720 MWh, reduces the annual equivalent number of cycles to 403.04 cycles/year, and achieves a higher annualized net income than M2. Although its annualized net income is lower than the static-depreciation estimate in M1, M3 provides a more realistic evaluation by incorporating the impact of operational intensity on lifetime and capacity-side depreciation.

(2) Under the benchmark parameters, S2 achieves the highest annualized net income, indicating that "leasing-based reliability support + passive accommodation + spot-market arbitrage" provides a better balance among revenue improvement, SOC-space utilization, and lifetime degradation. The selected spring representative day further shows that S2 coordinates price-driven arbitrage and passive accommodation by releasing SOC space before high-curtailment-risk periods and using idle leased resources for curtailed-energy accommodation. As a result, the potential curtailed-energy accommodation rate of this representative day increases from 5.54% in S1 to 99.59% in S2.

https://doi.org/10.3390/en19143311

(3) The passive-accommodation disabling test and sensitivity analysis show that passive accommodation plays an important role in reducing curtailed-energy penalties and improving annualized net income. Under variations in electricity price scaling, unit leasing prices, and curtailed-energy penalties, S2 maintains strong stability. When frequency-regulation compensation becomes high enough to offset the additional cycling degradation and dynamic-depreciation pressure, the preferred scheme may switch from S2 to S3. This indicates that the proposed model can identify the switching boundary of business strategies under different market compensation conditions.

It should be noted that the optimal configuration and preferred business scheme obtained in this paper are closely related to renewable energy output characteristics, grid-connection constraints, market prices, frequency-regulation compensation levels, and configuration boundary conditions. Therefore, they should not be directly interpreted as general capacity recommendations for all renewable energy bases. The main contribution of this paper is to establish an analytical framework that couples service boundaries, operational intensity, cycle-intensity-adjusted economic depreciation, and capacity configuration. The proposed depreciation mechanism should therefore be interpreted as a planning-level economic depreciation model based on annual equivalent cycles, rather than as a full electrochemical battery degradation model. Future research can further incorporate higher-resolution frequency-regulation response signals, more detailed state-of-health degradation models considering temperature, C-rate, variable depth-of-discharge ageing, and SOC-dependent calendar ageing, as well as broader cross-regional validation under different market mechanisms, grid-connection constraints, and planning-boundary assumptions.

Supplementary Materials: The following supporting information can be downloaded at: https://www.mdpi.com/article/10.3390/en19143311/s1, Supplementary Materials provides a simplified representative-day reproducibility dataset, covering seasonal representative-day renewable-output profiles, grid-connection limits, potential curtailed-energy profiles, spot-market price series, common parameter settings, and business-scheme settings.

Author Contributions: Conceptualization, Y.W., M.H. and T.X.; methodology, Y.W.; software, Y.W.; validation, Y.W., J.Z. and P.L.; investigation, Y.W.; resources, M.H. and T.X.; data curation, Y.W.; writing—original draft preparation, Y.W.; writing—review and editing, Y.W., J.Z., P.L., M.H. and T.X.; visualization, Y.W.; supervision, M.H. and T.X. All authors have read and agreed to the published version of the manuscript.

Funding: This research was funded by the Yunnan Provincial Science and Technology Talents and Platform Program, grant number 202105AD160042.

Data Availability Statement: The simplified representative-day reproducibility dataset and parameter tables used to reproduce the main case-study results are provided in Supplementary Materials. The original full-year renewable-energy output data, grid-connection constraint data, and part of the raw market-parameter data are available from the corresponding author upon reasonable request. Some raw project and third-party data are not publicly available due to project confidentiality and third-party data restrictions.

Conflicts of Interest: The authors declare no conflicts of interest.

Abbreviations

Symbol	Definition
SES	Shared energy storage
DBO	Dung Beetle Optimizer
MILP	Mixed-integer linear programming
IRR	Internal rate of return

S1	Leasing-based reliability support + passive accommodation of curtailed renewable energy
S2	Leasing-based reliability support + passive accommodation of curtailed renewable energy + spot-market arbitrage
S3	Leasing-based reliability support + passive accommodation of curtailed renewable energy + spot-market arbitrage + frequency-regulation ancillary services
M1	Static depreciation model
M2	Ex post dynamic depreciation evaluation model under a fixed configuration
M3	Dynamic depreciation closed-loop optimization model
P	Rated power of shared energy storage
E	Rated energy capacity of shared energy storage
N_{real}	Annual equivalent number of cycles
L_{real}	Actual economic lifetime
$C_{dep,real}$	Capacity-side dynamic depreciation cost
R_{lease}	Annual leasing revenue
R_{spot}	Annual spot-market arbitrage revenue
R_{freq}	Annual revenue from frequency-regulation ancillary services
C_{cur}	Annualized curtailed-energy penalty cost

Appendix A

Appendix A provides supplementary information supporting the case study and sensitivity analysis, including the typicality indicators of seasonal representative days, the settings of comparative models and business schemes, the service-reservation and supplementary-constraint parameters, representative-day SOC trajectories, and electricity-price-scaling sensitivity results.

Table A1. Probability coefficients and difference coefficients of seasonal typical scenarios.

Indicator	Spring Scenario	Summer Scenario	Autumn Scenario	Winter Scenario
Probability coefficient	0.2514	0.2514	0.2486	0.2486
Difference coefficient	0.2462	0.2527	0.2811	0.5011

Table A2. Business boundaries and main results of comparative cases.

Case ID	Leased Reserve Power/MW	Leased Reserve Energy Capacity/MWh	Upper Limit of Arbitrage-Available Power/MW	Frequency-Regulation Reserve Power/MW	Daily Passive Accommodation/MWh	Configuration Result P*/E*/(MW/MWh)	Annualized Net Income/(10^4 CNY·Year^{-1})
M1	61.20	170.56	100.80	—	—	180/533	4597.89
M2	61.20	170.56	100.80	—	—	180/533	4274.93
M3	61.20	230.40	100.80	—	139.86	180/720	4395.90
S1	72.00	64.80	—	—	7.78	180/180	1188.98
S2	61.20	230.40	100.80	—	139.86	180/720	4395.90
S3	50.40	197.10	90.00	8.10	127.40	180/657	3751.81
A1	61.20	230.40	100.80	—	139.86	180/720	4395.90
A2	61.20	203.20	100.80	—	—	180/635	3108.88

Note: A1 and A2 in the Case ID column denote passive-accommodation mechanism comparison cases and should not be confused with Table A1 or Table A2 in the Appendix A. An em dash (—) indicates that the corresponding service is not included in the case or that the value is not separately reported.

To support computational reproducibility, the detailed implementation settings of the DBO–MILP solution procedure are provided in Table A4.

Table A3. Parameter settings for service reservation and supplementary constraints.

Symbol	Value
$K_{lease,P}$	S1/S2/S3:0.40/0.34/0.28
$K_{lease,E}$	S1/S2/S3:0.36/0.32/0.30
K_{freq}	S1/S2/S3:0/0/0.045
γ	0.12
F_{test}	12 tests/year
DOD_{test}	0.02
$n_{maint,day}$	S1/S2/S3:0.12/0.16/0.22 cycles/day
ε	$10^{-6} \times 10^4$ CNY/MWh
K_P	1.10
K_E	1.10

Table A4. Computational implementation settings of the DBO–MILP solution procedure.

Category	Setting
Upper-level optimizer	Dung Beetle Optimizer (DBO)
Upper-level decision variables	Storage power capacity (P) and energy capacity (E)
Upper-level objective	Maximization of annualized net income
Population size	18
Maximum iterations/ termination criterion	30 iterations
Producer/breeder/thief ratios	0.20/0.30/0.20
Forager group	Remaining individuals
Stall probability	0.10
Capacity discretization	1 MW for (P), 1 MWh for (E)
Constraint handling	Boundary repair for (P), (E), and (E/P); penalty terms for investment-budget and annual-cycle-limit violations
Lower-level model	24 h mixed-integer linear programming (MILP) dispatch model
MILP solver	MATLAB intlinprog
MILP options	Display off; advanced heuristics; advanced cut generation; maximum time 60 s per MILP call
Big-M factor	1.0
Software environment	MATLAB R2022b, 64-bit Windows
Average computation time	75.81 s for the benchmark M3 stability runs

To evaluate the stability of the metaheuristic upper-level search, the benchmark M3 case was repeated for 10 independent DBO runs with different random seeds, and the results are reported in Table A5.

Table A5. Independent-run stability of the upper-level DBO search.

Run	Seed	P*/MW	E*/MWh	Annualized Net Income/ (10^4 CNY·Year^{-1})	N_{real}/ (Cycles·Year^{-1})	L_{real}/Year	Time/s
1	20260427	180	720	4395.9031	403.0446	14.8867	76.06
2	20260428	180	720	4395.9031	403.0446	14.8867	74.36
3	20260429	180	720	4395.9031	403.0446	14.8867	76.18
4	20260430	180	720	4395.9031	403.0446	14.8867	75.81
5	20260431	180	720	4395.9031	403.0446	14.8867	75.08
6	20260432	180	720	4395.9031	403.0446	14.8867	74.47
7	20260433	180	720	4395.9031	403.0446	14.8867	74.98
8	20260434	180	720	4395.9031	403.0446	14.8867	76.41
9	20260435	180	720	4395.9031	403.0446	14.8867	80.06
10	20260436	180	720	4395.9031	403.0446	14.8867	74.69

Note: The mean computation time is 75.81 s with a standard deviation of 1.67 s. The dominant configuration 180/720 MW/MWh appears in 100% of the independent runs, and the coefficient of variation of annualized net income is 2.18×10^{-14}%.

Table A6. Refined threshold analysis of the frequency-regulation compensation multiplier.

K_{FR}	S2 Net Income/ (10^4 CNY·Year^{-1})	S3 Net Income/ (10^4 CNY·Year^{-1})	$F_{S3}-F_{S2}$ (10^4 CNY·Year^{-1})	Preferred Scheme
3.50	4395.90	4352.30	−43.586	S2
3.55	4395.90	4364.30	−31.576	S2
3.60	4395.90	4376.30	−19.566	S2
3.65	4395.90	4388.30	−7.556	S2
3.70	4395.90	4400.40	4.454	S3
3.75	4395.90	4412.40	16.464	S3
3.80	4395.90	4424.40	28.475	S3
3.85	4395.90	4436.40	40.485	S3
3.90	4395.90	4448.40	52.495	S3
3.95	4395.90	4460.40	64.505	S3
4.00	4395.90	4472.40	76.515	S3

Note: The optimized S2 configuration remains P*/E* = 180/720 MW/MWh, while the optimized S3 configuration remains P*/E =180/657 MW/MWh over the refined scanning interval.

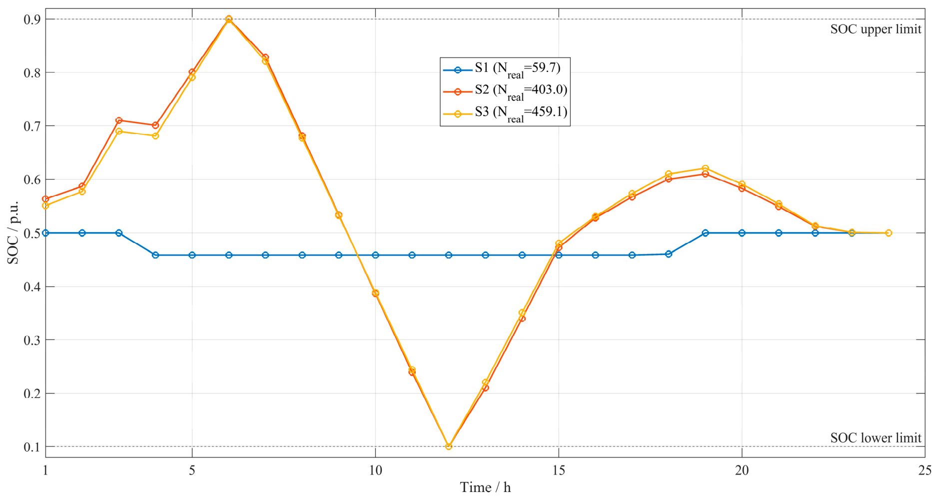

Figure A1. Representative-day SOC trajectories under different business schemes.

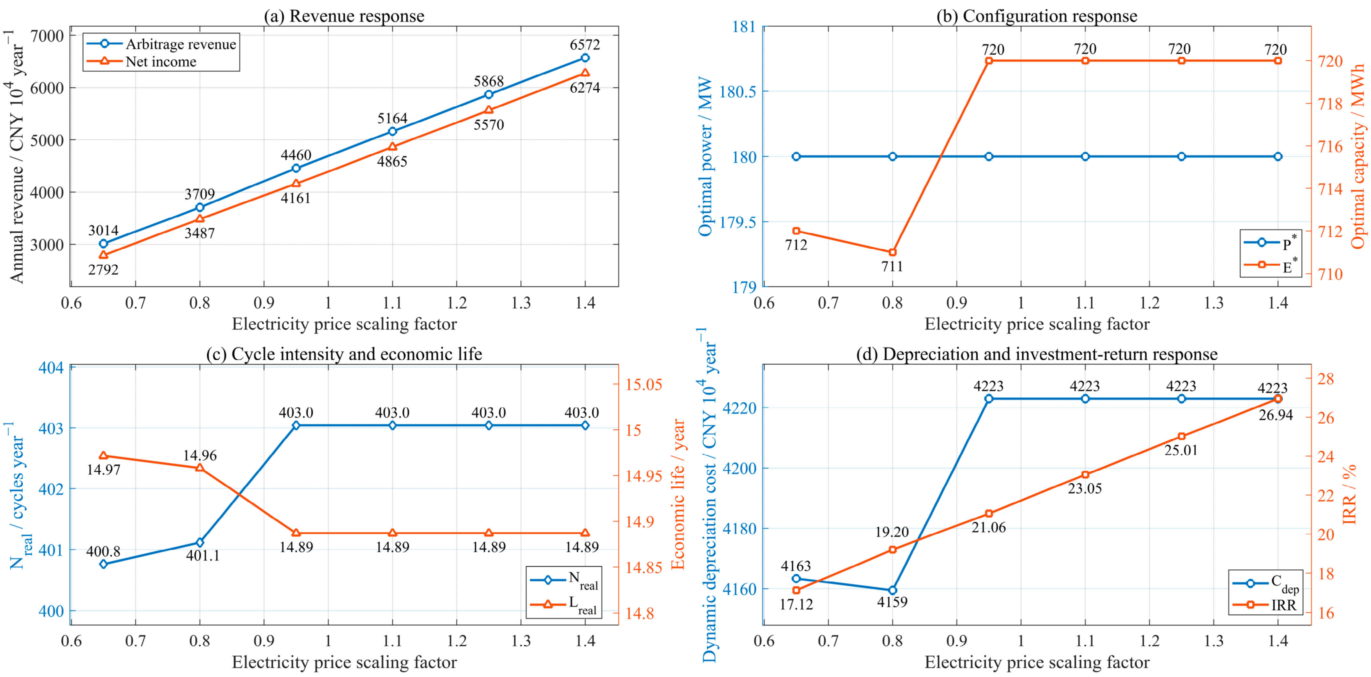

Figure A2. Effects of electricity price scaling on revenue, configuration, cycle life, and investment return.

References

1. Sayed, E.T.; Olabi, A.G.; Alami, A.H.; Radwan, A.; Mdallal, A.; Rezk, A.; Abdelkareem, M.A. Renewable Energy and Energy Storage Systems. *Energies* **2023**, *16*, 1415. [CrossRef]
2. Yuan, Z.; He, Y.; Meng, Z. Hybrid energy storage configuration methodology, taking into account the accumulation of wind farm forecast deviations. *Front. Energy Res.* **2024**, *12*, 1343879. [CrossRef]
3. Jafari, M.; Korpås, M.; Botterud, A. Power system decarbonization: Impacts of energy storage duration and interannual renewables variability. *Renew. Energy* **2020**, *156*, 1171–1185. [CrossRef]
4. Qiu, W.; Zhou, S.; Yang, Y.; Lv, X.; Lv, T.; Chen, Y.; Huang, Y.; Zhang, K.; Yu, H.; Wang, Y.; et al. Application Prospect, Development Status and Key Technologies of Shared Energy Storage toward Renewable Energy Accommodation Scenario in the Context of China. *Energies* **2023**, *16*, 731. [CrossRef]
5. Xiao, J.-W.; Yang, Y.-B.; Cui, S.; Liu, X.-K. A new energy storage sharing framework with regard to both storage capacity and power capacity. *Appl. Energy* **2022**, *307*, 118171. [CrossRef]
6. Khojasteh, M.; Faria, P.; Gomes, L.; Vale, Z. Energy trading strategy of community shared energy storage. *Electr. Eng.* **2024**, *106*, 3415–3426. [CrossRef]
7. Li, L.; Cao, X.; Zhang, S. Shared energy storage system for prosumers in a community: Investment decision, economic operation, and benefits allocation under a cost-effective way. *J. Energy Storage* **2022**, *50*, 104710. [CrossRef]
8. Han, O.; Ding, T.; Zhang, X.; Mu, C.; He, X.; Zhang, H.; Jia, W.; Ma, Z. A shared energy storage business model for data center clusters considering renewable energy uncertainties. *Renew. Energy* **2023**, *202*, 1273–1290. [CrossRef]
9. He, Y.; Xiao, J.-W.; Wang, Y.-W.; Liu, Z.-W.; He, S.-Y. Subjective-uncertainty-oriented dynamic renting framework for energy storage sharing. *Appl. Energy* **2025**, *378*, 124765. [CrossRef]
10. Lan, Z.; Hu, J.; Fang, X.; Qiu, W.; Li, J. Risk-based optimization for facilitating the leasing services of shared energy storage among renewable energy stations. *Front. Energy Res.* **2023**, *11*, 1286045. [CrossRef]
11. Liu, J.; Wu, J.; Lei, Z. Two-Stage Optimization Strategy for Market-Oriented Lease of Shared Energy Storage in Wind Farm Clusters. *Energies* **2025**, *18*, 2697. [CrossRef]
12. Miao, Y.; Chen, T.; Bu, S.; Liang, H.; Han, Z. Co-Optimizing Battery Storage for Energy Arbitrage and Frequency Regulation in Real-Time Markets Using Deep Reinforcement Learning. *Energies* **2021**, *14*, 8365. [CrossRef]
13. Pusceddu, E.; Zakeri, B.; Castagneto Gissey, G. Synergies between Energy Arbitrage and Fast Frequency Response for Battery Energy Storage Systems. *Appl. Energy* **2021**, *283*, 116274. [CrossRef]
14. Ellis, B.; White, C.; Swan, L. Degradation of Lithium-Ion Batteries That Are Simultaneously Servicing Energy Arbitrage and Frequency Regulation Markets. *J. Energy Storage* **2023**, *66*, 107409. [CrossRef]
15. Lee, J.-O.; Kim, Y.-S. Novel Battery Degradation Cost Formulation for Optimal Scheduling of Battery Energy Storage Systems. *Int. J. Electr. Power Energy Syst.* **2022**, *137*, 107795. [CrossRef]
16. Amini, M.; Khorsandi, A.; Vahidi, B.; Hosseinian, S.H.; Malakmahmoudi, A. Optimal Sizing of Battery Energy Storage in a Microgrid Considering Capacity Degradation and Replacement Year. *Electr. Power Syst. Res.* **2021**, *195*, 107170. [CrossRef]
17. Xue, J.; Shen, B. Dung Beetle Optimizer: A New Meta-Heuristic Algorithm for Global Optimization. *J. Supercomput.* **2023**, *79*, 7305–7336. [CrossRef]
18. Dou, Q.; Gao, X.; Wu, Y.; Chen, Y.; Xie, R.; Chen, J. A Multi-Level Coordinated Scheduling Strategy for Shared Energy Storage Systems under Electricity Spot and Ancillary Service Markets. *IET Renew. Power Gener.* **2024**, *18*, 3855–3868. [CrossRef]
19. Wang, Z.; Yang, S.; Xue, F.; Tan, Z.; Liu, W.; Ju, L. Robust Two-Level Market Coordinated Transaction Optimal Model and Benefit Allocation Strategy for a Novel Shared-Energy Aggregator. *IET Renew. Power Gener.* **2024**, *18*, 1535–1555. [CrossRef]
20. Yang, Y.; Chen, T.; Yan, H.; Wang, J.; Yan, Z.; Liu, W. Optimization Operation Strategy for Shared Energy Storage and Regional Integrated Energy Systems Based on Multi-Level Game. *Energies* **2024**, *17*, 1770. [CrossRef]
21. Cui, K.; Fan, K.; Zhao, Y.; Chi, M. Decentralized Micro-Energy Storage Capacity Sharing within the Residential Community: An Enhanced Uniform Price-Based Bidding Framework. *Front. Energy Res.* **2024**, *12*, 1409444. [CrossRef]
22. Wang, W.; Wang, H.; Sun, S.; Cao, G.; Wang, S.; Ji, Y. Optimal Configuration of Shared Energy Storage for Industrial Users Considering Lifetime and Charge-Discharge Strategy Coupling. *Front. Energy Res.* **2024**, *12*, 1510259. [CrossRef]
23. Zhang, L.; Yu, Y.; Li, B.; Qian, X.; Zhang, S.; Wang, X.; Zhang, X.; Chen, M. Improved Cycle Aging Cost Model for Battery Energy Storage Systems Considering More Accurate Battery Life Degradation. *IEEE Access* **2022**, *10*, 297–307. [CrossRef]
24. Collath, N.; Cornejo, M.; Engwerth, V.; Hesse, H.; Jossen, A. Increasing the Lifetime Profitability of Battery Energy Storage Systems through Aging Aware Operation. *Appl. Energy* **2023**, *348*, 121531. [CrossRef]
25. He, G.; Ciez, R.E.; Moutis, P.; Kar, S.; Whitacre, J.F. The Economic End of Life of Electrochemical Energy Storage. *Appl. Energy* **2020**, *273*, 115151. [CrossRef]
26. Mostafa, M.H.; Abdel Aleem, S.H.E.; Ali, S.G.; Ali, Z.M.; Abdelaziz, A.Y. Techno-Economic Assessment of Energy Storage Systems Using Annualized Life Cycle Cost of Storage (LCCOS) and Levelized Cost of Energy (LCOE) Metrics. *J. Energy Storage* **2020**, *29*, 101345. [CrossRef]

27. El Barkouki, B.; Laamim, M.; Rochd, A.; Chang, J.-W.; Benazzouz, A.; Ouassaid, M.; Kang, M.; Jeong, H. An Economic Dispatch for a Shared Energy Storage System Using MILP Optimization: A Case Study of a Moroccan Microgrid. *Energies* **2023**, *16*, 4601. [CrossRef]
28. Keske, C.; Srinivasan, A.; Sansavini, G.; Gabrielli, P. Optimal Economic and Environmental Arbitrage of Grid-Scale Batteries with a Degradation-Aware Model. *Energy Convers. Manag. X* **2024**, *22*, 100554. [CrossRef]
29. Dai, B.; Wang, H.; Li, B.; Li, C.; Tan, Z. Capacity Model and Optimal Scheduling Strategy of Multi-Microgrid Based on Shared Energy Storage. *Energy* **2024**, *306*, 132472. [CrossRef]
30. Gu, M.; Song, H.; Liu, C.; Meegahapola, L.; Jalili, M.; Yu, X.; Dickson, G. Large-Scale Battery Inverter and Energy Capacity Sizing for Frequency Control Ancillary Services with High Share of Solar-PV Generation: A Data-Driven Approach. *IET Energy Syst. Integr.* **2025**, *7*, e70003. [CrossRef]
31. Liang, Y.; Zhou, M.; Bai, X.; Wang, Z.; Cao, Y.; Wang, X.; Zhu, R.; Zhang, W. Capacity Compensation Mechanism Design for Energy Storage Sharing in New Energy Base. *IET Renew. Power Gener.* **2025**, *19*, e70059. [CrossRef]
32. Zhou, S.; Wu, W.; Sun, Y.; Zhang, Y.; Li, Y.; Zheng, X.; Su, X. Energy Storage Configuration and Benefit Evaluation Method for New Energy Power Plants Based on Game Theory. *J. Electr. Eng. Technol.* **2025**, *20*, 1959–1973. [CrossRef]
33. Khan, I.U.; Jamil, M. Energy Arbitrage Analysis for Market-Selection of a Battery Energy Storage System-Based Venture. *Energies* **2025**, *18*, 4245. [CrossRef]
34. Zhao, C.; Andersen, P.B.; Træholt, C.; Hashemi, S.; Kerekes, T. Grid-Connected Battery Energy Storage System: A Review on Application and Integration. *Renew. Sustain. Energy Rev.* **2023**, *182*, 113400. [CrossRef]
35. Ma, Q.; Wei, W.; Mei, S. Health-Aware Coordinate Long-Term and Short-Term Operation for BESS in Energy and Frequency Regulation Markets. *Appl. Energy* **2024**, *356*, 122363. [CrossRef]